

1 Evaluation of WRF and CHIMERE models for the simulation 2 of PM_{2.5} in large East African urban conurbations.

3 Andrea Mazzeo^{1,2}, Michael Burrow¹, Andrew Quinn¹, Eloise A. Marais³, Ajit Singh², David
4 Ng'ang'a⁴, Michael J. Gatari⁴, and Francis D. Pope²

5 1. School of Civil Engineering, University of Birmingham, Birmingham UK

6 2. School of Geography Earth and Environmental Sciences – GEES, University of Birmingham, Birmingham
7 UK

8 3. Department of Geography, University College London, London, UK.

9 4. Institute of Nuclear Science and Technology, University of Nairobi, Nairobi, Kenya

10

11 Correspondence to Andrea Mazzeo (a.mazzeo@bham.ac.uk)

12 **Abstract:** Urban conurbations of East Africa are affected by harmful levels of air pollution. The paucity of local
13 air quality networks and the absence of capacity to forecast air quality make difficult to quantify the real level of
14 air pollution in this area. The chemistry-transport model CHIMERE has been used *along* with the meteorological
15 model WRF to run simulations at high spatial resolution (*2x2 km*) of hourly concentrations of Particulate Matter
16 PM_{2.5} for three East African urban conurbations: Addis Ababa in Ethiopia, Nairobi in Kenya, and Kampala in
17 Uganda. Two existing emission inventories were combined to test the performance of CHIMERE as an air quality
18 *model* for a target monthly period of 2017 and the results compared against observed data from urban, *roadside*,
19 and rural sites. The results show that the model is able to reproduce hourly and daily temporal variability of
20 aerosol concentrations close to observations in urban, roadside and in rural environments. CHIMERE's
21 performance as a tool for managing air quality was also assessed. The analysis demonstrated that despite the
22 absence of high-resolution data and up-to-date biogenic and anthropogenic emissions, the model was able to
23 reproduce 66 – 99% of the daily PM_{2.5} exceedances above the WHO 24-hour mean PM_{2.5} guideline (25 µg m⁻³) in
24 the three cities. An analysis of the 24-hour average levels of PM_{2.5} was also carried out for 17 constituencies in
25 the vicinity of Nairobi. This showed that 47% of the constituencies in the area exhibited *poor* air quality index for
26 PM_{2.5} in the unhealthy category for human health exposing between 10,000 to 30,000 people/km² to harmful level
27 of air contamination.

28

29 **Keywords:** Air quality, East Africa, Particulate Matter, Anthropogenic emissions, numerical modelling, Air
30 Quality Index

31

32 1 Introduction

33

34 The world's population has grown rapidly by 1 billion people in the last 12 years, reaching 7.9 billion in 2021.

35 *The World Population Prospects (WPP) made by the United Nations (U.N.)* suggest a continuing annual increase
36 of 1.8%, meaning the global population will reach 8.5 billion by 2030, 9.7 by 2050, and 11.2 by 2100 (UN-WPP,
37 2019). The African continent is predicted to have the fastest growing population rate in the world, and it is
38 projected to double between 2010 and 2050, surpassing two billion (UN-WPP, 2019). In addition to this a 60%
39 increase in population has been predicted by 2050, specifically in urban areas (UN-WPP, 2019).

40

Deleted: tool

Deleted: a

Deleted: low

Deleted: ¶

Deleted: Future projections

Deleted: (WPP, 2015)

Deleted: (WPP, 2011)

Deleted: (WPP, 2012).

49 Population in Sub-Saharan East African (SSEA) countries have increased drastically ~~from~~ 1991 to 2019. In that
50 period of time and according to data from the World Bank database ~~(WB, 2022)~~, the Kenyan population grew
51 from 24 to 52 million, the Ugandan population from 17 to 44 million and the Ethiopian population from 50 to 112
52 million. These increases in population were accompanied by a similar rate of increase in road transport, industrial
53 activities and in the use of solid fuels (e.g., woods, charcoal, and agricultural residues) for cooking purposes in
54 urban areas (Bockarie et al., 2020;Marais et al., 2019).

Deleted: since

Deleted:

Deleted: (WB, 2022)

55
56 As a result of these population increases, air quality of the urban areas of these countries, historically influenced
57 by the large presence of seasonal burning biomass emissions (Haywood et al., 2008;Lacaux, 1995;Lioussé et al.,
58 2010;Thompson A. M., 2001), is progressively degrading (Marais and Wiedinmyer, 2016). This, in combination
59 with the expanding urban population, has greatly increased the exposure of citizens to harmful Particulate Matter
60 (PM) pollution with an aerodynamic diameter smaller than 10 and 2.5 μm (PM₁₀ and PM_{2.5}, respectively) (Gatari
61 et al., 2019;Kinney et al., 2011;Li et al., 2017;UN-Habitat, 2017).

62
63 Several diseases have been attributed to PM exposure in SSEA, including cardiovascular and cardiopulmonary
64 diseases, cancers, and respiratory deep infections (Dalal et al., 2011;Mbewu, 2006;Parkin et al., 2008). In 2012,
65 the World Health Organization (WHO) estimated ~~176,000~~ deaths in SSEA were directly connected to air pollution
66 (WHO, 2012). Modelling studies have also found that exposure to outdoor air pollution has led to 626,000
67 disability-adjusted life per year (DALYs) in SSEA alone (Amegah and Agyei-Mensah, 2017), highlighting that
68 these numbers could be much higher considering the limited amount of air quality data emanating from the region
69 that are available for research purposes.

Deleted: that in 2012

70
71 Considering the likely severe impacts of air pollution on human health in SSEA, the research interest in
72 understanding air pollution trends in East Africa has increased in recent years. Many researchers have analysed
73 the levels of contamination by short-term measurement campaigns (Amegah and Agyei-Mensah, 2017;deSouza
74 P., 2017;Egondi et al., 2013;Gaita et al., 2014;Gatari et al., 2019;Kume, 2010;Ngo et al., 2015;Pope et al.,
75 2018;Schwander et al., 2014;Vliet, 2007;Singh et al., 2021). Other studies observed annual average PM_{2.5}
76 concentrations in the order of 100 $\mu\text{g m}^{-3}$ quantified in a small number of urban areas of SSEA (Brauer et al.,
77 2012). These levels are about four times higher than the 24-hour average and ten times higher than the annual
78 average WHO guidelines for PM_{2.5} (Avis W. and Khaemba W., 2018;WHO, 2016) and underline that air pollution
79 is a serious problem in this area of the world. A recent study by Singh et al. (2020), using visibility as a proxy for
80 PM, showed that air quality in Addis Ababa, Kampala and Nairobi has degraded alarmingly over the last 4
81 decades.

82
83 The lack of long-term air quality monitoring networks in many African countries have made it difficult to have
84 reliable long-term air quality data (Petkova, 2013;Pope et al., 2018;Singh et al., 2020) and still little is known
85 about the levels of air contamination in large urban conurbations ~~(Burroughs Peña and Rollins, 2017)~~. The paucity
86 and sometimes complete absence of reliable data on air pollution levels makes it difficult to quantify the magnitude
87 of the problem. Consequently, it is difficult for local and national authorities to plan possible improvement
88 measures for the mitigation of anthropogenic emissions. Even if important steps forward have been made to

Deleted:

Deleted: (Peña, 2017)

95 improve the knowledge relative to anthropogenic emissions and emission inventories for Africa used for
96 numerical simulations and forecasts of air quality (Assamoi and Lioussé, 2010; Lioussé, 2014; Marais and
97 Wiedinmyer, 2016) the lack of surface observations to validate the emission magnitude and the simulated
98 concentrations make these inventories susceptible of large error.

99
100 In this work we test a meteorological and a chemistry-transport model (CTM) to simulate the hourly urban and
101 rural levels of PM_{2.5} in [three SSEA urban conurbations](#) during a monthly period of 2017. We present the results
102 of the validation of both models for the capital cities of Kenya, (Nairobi), Ethiopia (Addis Ababa) and Uganda
103 (Kampala) against observation data. For Nairobi, we compare model outputs with observations from rural and
104 roadside sites observations collected during the “A Systems approach to Air Pollution in East Africa” research
105 project (ASAP-East Africa - www.asap-eastafrica.com, hereafter called ASAP) (Pope et al., 2018). For Addis
106 Ababa and Kampala, the model was validated using hourly observations of PM_{2.5} collected by the respective U.S.
107 Embassies.

108
109 Moreover, we assess the suitability of the CTM as a decision support tool for policy makers to plan possible
110 mitigation policies oriented to quantify the real level of air pollution in urban areas and quantify the human
111 exposure to PM_{2.5}. Specifically, in terms of the accuracy of the model, ~~we estimate~~ the daily WHO threshold limit
112 exceedances of PM_{2.5} in the three urban conurbations. Finally, for the particular case of Nairobi, we evaluate the
113 average air quality indices by local constituency for the whole analysed period giving a new insight of the real
114 level of air contamination in Nairobi to the general public and the relative population exposed to harmful level of
115 air contamination.

117 2 Material and Methods

118
119 [The meteorological and chemistry-transport models used in this work have been configured to simulate hourly
120 weather parameters and concentrations of PM_{2.5} using available input data for the simulations and observations
121 from the real world for the validation. The availability of the observations for the validation of both models comes
122 from different providers, have different frequency in time and, in the case of PM_{2.5} observations, come from
123 different environments \(rural, urban, roadside sites\). No vertical observations were available for the validation of
124 both models.](#)

126 2.1 Meteorological model WRF

127
128 The Weather Research and Forecasting (WRF) model is a numerical model for weather predictions and
129 atmospheric simulations and is used commercially and for research purposes, including by the US National
130 Oceanic and Atmospheric Administration (Powers, 2017; Skamarock, 2008).

131
132 [WRF was used to drive the meteorology for CHIMERE using three geographical domains at different resolutions
133 \(from 18×18 km to 2×2 km\) vertically divided into 30 levels, nine of which are below 1500 m. The first external
134 domain has a spatial resolution of 18×18 km \(Figure 1\), with three nested domains at a resolution of 6×6 km](#)

Deleted: in

Deleted: ing

Deleted: The models have worked on a system of 3 geographical domains at different resolution aimed to run simulation of atmospheric chemistry at 2×2 km of spatial resolution for the first time in this area of the world. ¶

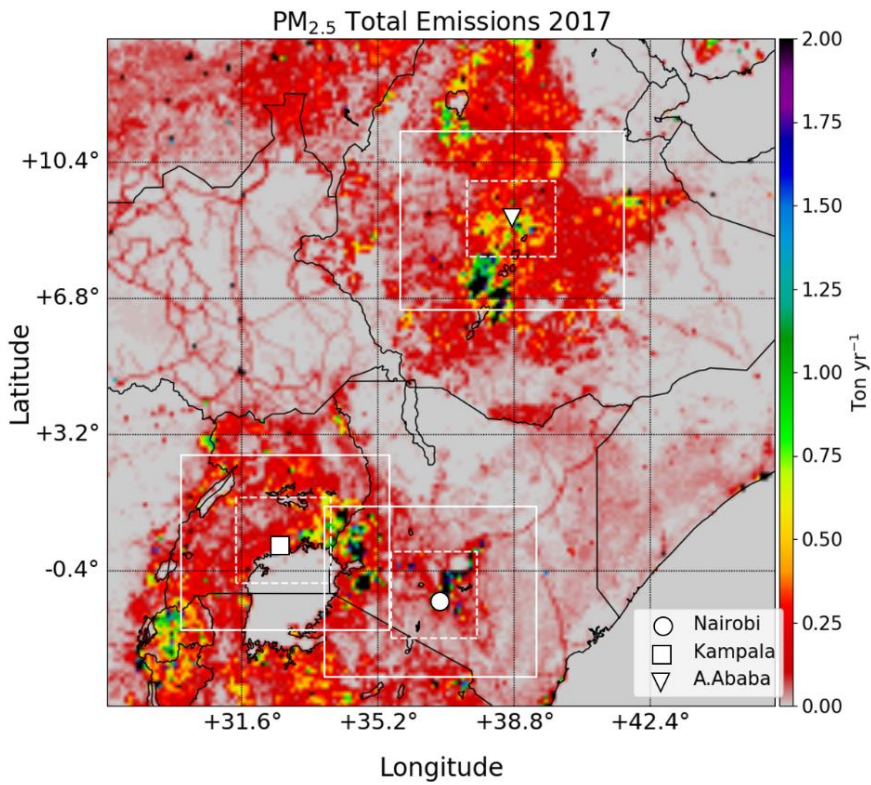
Deleted: s

Deleted: s

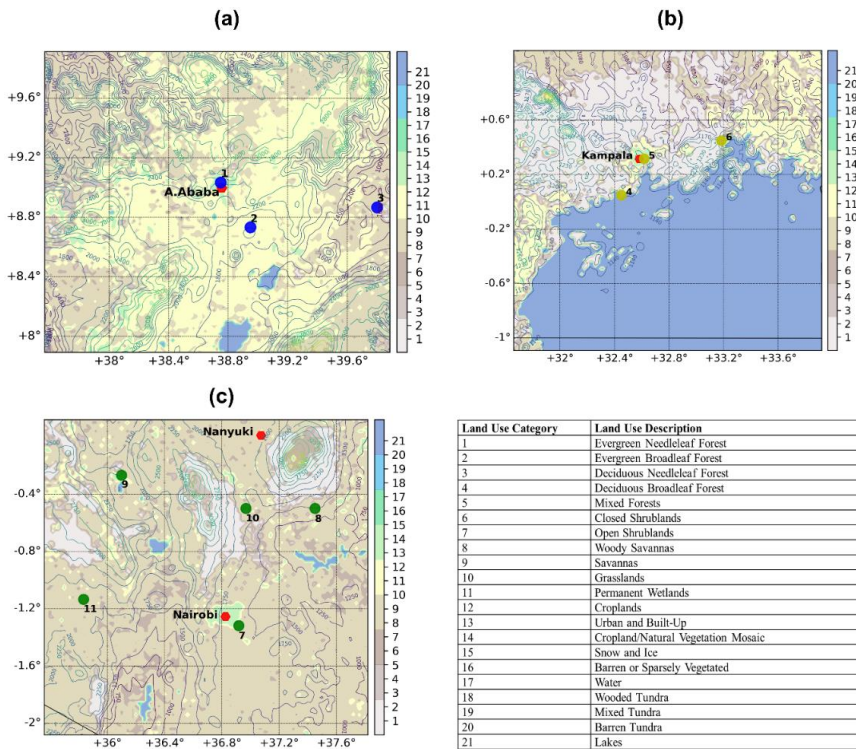
144 centred on the three countries of interest (Figure 1, white squares). Three further nested domains with a resolution
145 of 2x2 km centred on Addis Ababa, Kampala, and Nairobi (Figure 1, white dashed squares, and Figure 2) are the
146 focus of the analysis.

Deleted: 3

Deleted: a, b, c



147
148 **Figure 1:** Spatial distribution of the $PM_{2.5}$ emissions from DICE-EDGAR merged emission inventory for East Africa for the
149 WRF domain at 18×18 km of resolution. The continuous white lines show the location of the first nested domain at 6×6 km of
150 resolution used in WRF-CHIMERE. The dashed white squares give the locations of the second nested domains at 2×2 km
151 centred on Addis Ababa (Ethiopia, white triangle), Kampala (Uganda, white square) and Nairobi (Kenya, white circle) used
152 for WRF-CHIMERE.



155
 156 **Figure 2:** Second-nested domains at a spatial resolution of 2×2 km centred on the cities of Addis Ababa (ETH2K - a), Kampala
 157 (UGA2K - b), Nanyuki and Nairobi (KEN2K - c) created using the WRF model outputs. The red dots represent locations of
 158 PM_{2.5} measurements. The blue, yellow, and green dots refer to the location of the ground weather stations used for the
 159 meteorological validation in Ethiopia, Uganda, and Kenya, respectively. The numbers relate to the stations detailed in Table
 160 2. Contour lines are relative to the height meters from the ground levels from WRF outputs while the colour scale applied to
 161 the maps a, b and c represents the 21 classes of classification of the land use adopted in WRF simulations. The description of
 162 each land use category is provided in the legend.

Deleted: ¶

163
 164 The configuration adopted for the WRF simulations has been chosen according to previous works made on East
 165 Africa (Kerandi et al., 2016; Kerandi et al., 2017; Pohl et al., 2011) and is summarized in Table 1. The Yonsei
 166 University Scheme (YSU - (Hong S., 2006)) was chosen to represent the Planetary Boundary Layer while the
 167 Community Atmosphere Model (CAM - (Collins, 2004)) was used for the long and short-wave radiation scheme.
 168 Initial and boundary conditions for the external coarse domain at 18×18 km were obtained from the NCEP FNL
 169 (Final) Operational Global Analysis data (Wu, 2002). Boundary condition for the first (6×6 km) and second (2×2
 170 km) nest domains were taken from the respective parent domains using the two-way-nesting approach. The
 171 process enables the lateral conditions for the internal domains to be calculated from the outputs of the respective
 172 parent domains at lower resolution at every time step of the simulation.
 173

175 The land use option chosen for the simulations was NOAH (Tewari, 2004) while the WRF Single-moment 3-
176 class Scheme (WSM3) for clouds and ice proposed by Hong S. (2004) was chosen for the reproduction of the
177 microphysical processes in WRF.

178

179 2.2 The Chemistry Transport model CHIMERE

180

181 CHIMERE, version 2017r4 (Mailler et al., 2017), is a Eulerian numerical model for reproducing three-
182 dimensional gas-phase chemistry and aerosols processes of formation, dispersion, wet and dry deposition over a
183 defined domain with flexible spatial resolutions. CHIMERE has been used for a number of comparative research
184 studies of Ozone and particulate matter PM₁₀ from the continental scale, (Bessagnet et al., 2016; Zyryanov et al.,
185 2012) to the urban scale (van Loon et al., 2007; Vautard et al., 2007; Mazzeo et al., 2018). Furthermore, the model
186 has been used for event analysis, scenario studies (Markakis et al., 2015; Trehela et al., 2019), forecasts, and
187 impact studies of the effects of air pollution on health (Valari and Menut, 2010) and vegetation (Anav et al., 2011).
188 The authors highlight that the version of CHIMERE adopted is the 2017r4, the most recent available at the time
189 when the present work was realized.

190

191 [CHIMERE model has been used to simulate the first nested domains at 6×6 km and the second nested domains at](#)
192 [2×2 km of spatial resolution. The configuration adopted in this work uses initial and boundary conditions from](#)
193 [the global three-dimensional chemistry-transport model \(LMDz-INCA, Hauglustaine et al. \(2004\)\), both for](#)
194 [gaseous pollutants and for aerosols for the most external domain at 6×6 km of resolution while for the most](#)
195 [internal domains at 2×2 km of resolution, the boundary conditions are calculated from model outputs of the parent](#)
196 [domains. The complete chemical mechanism used for all the simulations was SAPRC-07-A \(Carter, 2010\) which](#)
197 [can describe more than 275 reactions of 85 species. SAPRC-07-A is the most recent chemical mechanism](#)
198 [available for CHIMERE version 2017r4.](#)

199

200 Horizontal and vertical diffusion is calculated using the approach suggested by Van Leer (1979) and the
201 thermodynamic equilibrium ISORROPIA model (Nenes, 1998) is used for the particle/gases partitioning of semi-
202 volatile inorganic gases. The model permits calculation of the thermodynamical equilibrium between sulphates,
203 nitrates, ammonium, sodium, chloride and water dependent upon temperature and relative humidity data.

204

205 [Dry and wet deposition is calculated in CHIMERE. The particle dry deposition velocities are calculated as a](#)
206 [function of particle size and density as well as relevant meteorological variables, including deposition processes,](#)
207 [such as, turbulent transfer, Brownian diffusion, impaction, interception, gravitational settling and particle rebound](#)
208 [\(Zhang et al., 2001\). Wet deposition is described modelled using a first-order decay equation as described in](#)
209 [Loosmore and Cederwall \(2004\).](#)

210

211 Radiative transfer processes are accounted in CHIMERE using the Fast-JX model (Wild, 2000; Bian, 2002). Fast-
212 JX is applied also in other models (Voulgarakis, 2009; Real and Sartelet, 2011; Telford et al., 2013). The photolysis
213 rates calculated by Fast-JX model are validated both inside the limits of the boundary layer (Barnard, 2004) and
214 in the free troposphere (Voulgarakis, 2009).

Deleted: CHIMERE

Deleted:

Deleted: are

Deleted:

219
 220 Secondary organic aerosols (SOAs), including biogenic and anthropogenic precursors, [are](#) modelled in CHIMERE
 221 as described by (Pun, 2006). SOAs formation is represented as a single-step oxidation of the precursors,
 222 differentiating hydrophilic by hydrophobic SOAs in the partitioning formulation. Finally, biogenic emissions were
 223 taken in account within CHIMERE using MEGAN model outputs as described by (Guenther, 2006).
 224

225 **Table 1:** Main configuration parameters adopted for the modelling system WRF-CHIMERE for all simulations.

WRFv3.9.1 Configuration		
Initial and Boundary conditions	GFS FNL- Reanalysis	Wu (2002)
PBL Parametrization	YSU	Hong S. (2006)
SW/LW Radiation Scheme	CAM	Collins (2004)
Land Use	NOAH	Tewari (2004)
Micro Physics Scheme	WSM3	Hong S. (2006)
Vertical Levels	30	
CHIMERE2017r4 Configuration		
Initial and boundary conditions	LMDz-INCA	Hauglustaine et al. (2004)
Anthropogenic Emissions	EDGARv3.4.1 + DICE-Africa	Crippa M. (2018); Marais and Wiedinmyer (2016)
Biogenic Emissions	MEGAN	Guenther (2006)
Gas/Aerosol Partitions	ISORROPIA	Nenes (1998)
Secondary Organic Aerosols	1	Pun (2006)
Radiative Transfer	Fast-JX	Wild (2000); Bian (2002)
Chemistry Mechanism	SAPRC-07-A	Carter (2010)
Horiz. / Vert. Transport scheme	VanLeer	Van Leer (1979)
Vertical Levels	30	

Formatted Table

226
 227 **2.3 Emission Inventories**
 228

229 [To correctly describe the impact of anthropogenic emissions on urban air quality of Nairobi, Kampala and Addis](#)
 230 [Ababa, industrial and on-grid power generation emissions from the Emissions Database for Global Atmospheric](#)
 231 [Research inventory \(hereafter EDGAR, version 3.4.1\) \(Crippa M., 2018\) were combined with non-industrial,](#)
 232 [prominent combustion sources from the Diffusive and Inefficient Emission inventory for Africa \(hereafter DICE\)](#)
 233 [\(Marais and Wiedinmyer, 2016\).](#)
 234

Deleted: are

235 EDGAR is a global inventory developed for year 2012 and DICE is a regional inventory for 2013. DICE includes
 236 important sources in Africa (e.g., motorcycles, kerosene use, open waste burning, and *ad hoc* oil refining, among
 237 others) that are absent or misrepresented in global inventories. Both inventories represent the most up-to-date
 238 anthropogenic emissions available for East Africa at the time of [the](#) air quality model was used for this work. Both
 239 inventories have spatial resolution of 0.1×0.1° and provide annual total of anthropogenic emissions for relevant
 240 gases and aerosols.

241
 242 On one hand, EDGAR provides emissions data for CO, NO, NO₂, SO₂, NH₃, NMVOCs, BC, OC, PM₁₀ and PM_{2.5}
 243 as [annual totals](#) divided by the sector according to the IPCC-1996 classification. All human activities with
 244 exception of large-scale biomass burning are included in EDGAR (Crippa M., 2018). On the other hand, DICE
 245 provides emissions from particular diffuse and inefficient combustion emission sources (e.g., road transport,

Deleted: an

248 residential biofuel use, energy production and charcoal production and use) for gaseous pollutants (CO, NO, NO₂,
249 SO₂, NH₃, NMVOCs) and aerosols (BC, OC). Seasonal biomass burning that is considered a large pollution source
250 in Africa is included in DICE as comparable emissions of black carbon (BC) and higher emissions of nonmethane
251 volatile organic compounds (NMVOCs). Emissions from DICE were used to provide annual total emissions for
252 particular emission sources considered to be misrepresented or missing in a global inventory such as EDGAR.
253

254 The preparation of the final emission inventory was carried out in two steps. First, DICE and EDGAR inventories
255 were merged, by pollutant and by sector, following the approach suggested by Marais and Wiedinmyer (2016).
256 PM_{2.5} emissions are included in DICE as individual components of organic carbon (OC) and black carbon (BC)
257 but they need to be expressed as lumped PM_{2.5} in CHIMERE. Therefore PM_{2.5} was calculated as the sum of
258 Organic Carbon (OC - originally present in DICE) multiplied with a conversion factor ($c = 1.4$) following Pai et
259 al. (2020) to represent Organic Aerosols emissions and summed with Black Carbon (BC – originally present in
260 DICE) as follows:

$$PM_{2.5} = (OC \times c) + BC$$

Eq. (1)

261
262
263
264 Secondly, the emisurf2016 pre-processor of CHIMERE was used to scale the emissions from the original
265 resolution of 0.1×0.1° (~10 km) to the final resolution of each domain simulated (6×6 and 2×2 km) using
266 population density data provided from the Socioeconomic Data and Application Centre (SEDAC)
267 (<http://sedac.ciesin.columbia.edu/>) as proxy for the spatial distribution. SEDAC provides population density maps
268 at high resolution (1×1 km) for the years 2010, 2015 and 2020. The SEDAC population density data calculated
269 for most internal domains at 2×2 km (Figure 2) suggest for 2010 a total population of 7 million for Nairobi, 4.8
270 million for Kampala and 4.5 million for Addis Ababa. These totals grow respectively to 8.1, 5.9 and 5.0 million
271 for 2015 and to 9.4, 7.3 and 5.7 million for 2020. The original SEDAC data were used for a linear extrapolation
272 of the population density data to the target year 2017 and were used by emisurf2016 for the spatial allocation of
273 the emissions. [Additionally, emisurf2016 permitted to temporally distribute the original total annual emissions
274 rates according to seasonal, weekly, and daily variation profiles.](#) The resulting merged inventory (hereafter, DICE-
275 EDGAR) totals by pollutant and sectors for the most external domain at 18×18 km of resolution are shown in
276 Figure 3.

277
278 Biogenic emissions and mineral dust considered in this work have been calculated in-line by CHIMERE. The
279 former are calculated by MEGAN model outputs as described by Guenther (2006) while the latter are calculated
280 using the USGS land use database provided by CHIMERE. The soil is represented by relative percentages of sand,
281 silt, and clay for each model cell. The USGS database, called STATSGO-FAO accounts of 19 different soil types
282 recorded in the global database with native resolution of 0.0083×0.0083°. To have homogeneous datasets, the
283 STATSGO-FAO data are re-gridded into the CHIMERE simulation grids. For mineral dust emission calculations,
284 the land use is typically used to provide a desert mask specifying what surface is potentially erodible.
285

Deleted:)

Deleted: for

Formatted: Font: Italic

Formatted: Space After: 8 pt

Formatted: Line spacing: 1.5 lines

Formatted: Space After: 8 pt

Deleted: 3a, b, c

Deleted: 2

The emissions used in this work might not reflect the true values due to missing emission sources and the mismatch of the simulated time period and the date of the emission inventories. The lack of up-to-date national emission inventories collected at a sufficient resolution, in addition to the lack of research sources providing projections of emissions for 2017, meant that it was not possible to generate more detailed information about the anthropogenic sources of emissions for East Africa.

Deleted: The emissions used in this work could still potentially not account for additional misrepresented or unaccounted sources due to the time difference between the age of the data in the EDGAR and DICE inventories and the observations used for the validation of the modelling system.

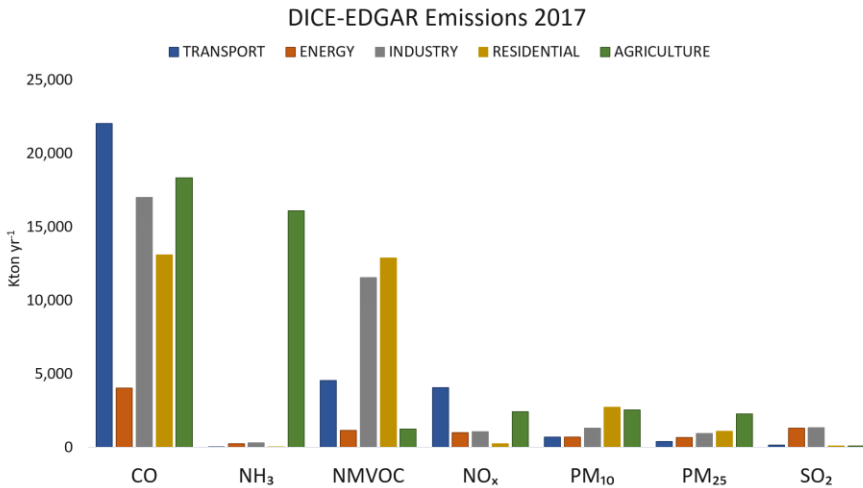


Figure 3: Annual Totals for the merged emission inventory DICE-EDGAR for year 2017 calculated on the spatial domain at 18×18 km shown in Figure 1.

Deleted: 2

It is noted that the time stamp of the anthropogenic emissions and the validation period are different. The emissions are relative to year 2013 while the observation used for the validation for 2017. In the absence of additional data and in the lack of national or local mitigation policies in the three countries we assume that the differences in time stamp do not make large difference to the emission estimates. More detailed analysis of the emission sources and the implementation of possible mitigation policies at national and local levels could in future change this situation.

Finally, we recall that one of the main objectives of the present work is to evaluate the performance of WRF and CHIMERE models in reproduce meteorology and air pollution levels in urban conurbation_s using the most-up-to-date available data and giving in this way a new insight on the state of the art of the numerical modelling for air quality in this area of the world highlighting possible improvements for future works.

Deleted: objective

2.4 Weather and Chemistry Observations

WRF and CHIMERE models have been validated for a limited monthly period between the 14th of February and 14th of March 2017. The choice of this period is because of the availability of continuous measurements for the validation of both models. While for the case of WRF observations with frequency variable from 3 to 6 hours are available from the UK Met Office MIDAS database (MetOffice, 2012) for different locations, rarer are PM_{2.5}

observations that last over one month with a measurement frequency of one hour, [and from different environments \(e.g., rural, urban, or roadside sites\)](#).

The period chosen for the simulations of meteorology has to be representative of the average weather conditions of the analysed area and avoid unusual weather conditions (e.g., extreme events) that could impact the physical and chemical processes described in the CTM and affect the final concentrations of secondary pollutants simulated. The February to March time period in East Africa does not have extreme temperatures (mean temperatures approximately 10 - 25°C according to the country) and little rainfall that could affect the observations of weather conditions and PM_{2.5} concentrations (USAID, 2022). These conditions and the absence of alternative data covering a large time frame for the validation of CHIMERE have constrained the period of simulation to the present period.

Table 2: UK Met Office ground weather stations used for the validation of the 2×2km domains. Station n_i corresponds to the position of each station in Figure 2a, b and c and PM_{2.5} observation points for the urban domains of Addis Ababa, Kampala and Nairobi used for the validation of CHIMERE model.

Station n.	Domain	Name	Latitude	Longitude	Elevation
1	ETH2K	Addis – Bole	0.03° N	38.75° E	1900 m
2		Harar Meda	8.73° N	38.95° E	2355 m
3		Metehara	8.87° N	39.90° E	930 m
		U.S. Embassy (PM _{2.5} – urban background)	9.05° N	38.76° E	1900 m
4	UGA2K	Entebbe (Airport)	0.05° N	32.45° E	1155 m
5		Kampala	0.32° N	32.62° E	1144 m
6		Jinja	0.45° N	33.18° E	1175 m
		U.S. Embassy (PM _{2.5} – urban background)	0.30° N	32.59° E	1150 m
7	KEN2K	Nairobi (Airport)	1.32° S	36.92° E	1624 m
8		Embu	0.50° S	37.45° E	1493 m
9		Nakuru	0.27° S	36.10° E	1901 m
10		Nyeri	0.50° S	36.97° E	1759 m
11		Narok	1.13° S	35.83° E	2104 m
	Tom Mboya Street (PM _{2.5} – roadside)	1.28° S	36.82° E	1795 m	
	Nanyuki (PM _{2.5} – rural background)	0.01° N	37.07° E	1947 m	

Observations of temperature, wind speed and directions used for the validation of WRF were taken from the UK Met Office MIDAS database. Data from 11 weather stations, three for the domain of Ethiopia (hereafter ETH2K, Figure 2a) and Uganda (hereafter UGA2K, Figure 2b) and five for the domain of Kenya (hereafter KEN2K, Figure, 2c) were used to validate the simulations at a resolution of 2×2 km (Table 2).

The ground stations are at different altitudes above sea level to a maximum of 2355 m (e.g., the Harar Meda station in Ethiopia, n₂ in Figure 2a). The validation was performed by comparing model outputs with observations for the variables, namely surface temperature, wind speed and direction and relative humidity. The latter, not originally available in the MIDAS dataset, was calculated using the coefficients proposed by Alduchov O. (1996) based on hourly surface and dew point temperatures observed values and then compared with modelled data obtained by WRF.

Deleted: ¶
Moreover, the options chosen for the configuration of the meteorology and chemistry-transport models can result in better performance in a season more than in another according to the combination of weather and chemical parameters chosen for both models.

Deleted: MIDAS

Deleted: °

Deleted: 3

Formatted Table

Deleted: (°)

Deleted: (°)

Deleted: . (m)

Formatted: Font: Not Bold

Deleted: -

Formatted: Font: Not Bold

Formatted: Font: Not Bold

Formatted: Font: Not Bold

Formatted: Font: Not Bold

Deleted: (UK, 2012)

Deleted: 3

Deleted: 3

Deleted: 3

Deleted: .

Deleted: 3

Hourly concentrations of PM_{2.5} were used for the validation of CHIMERE for the three internal domains at 2×2 km (Figure 2). For the city of Nairobi, data from roadside background site located at Tom Mboya Street was used (1.28° S, 36.82° E), while data from the rural background were provided by a site located in Nanyuki, Kenya (0.01° N, 37.07° E). Both the field sites data were obtained from the field sampling campaign performed by Pope et al., (2018). For the urban background locations of Addis Ababa and Kampala, hourly concentration of PM_{2.5} were obtained from the air quality monitoring stations of the two U.S. Embassies in Ethiopia (9.05° N, 38.76° E) and Uganda (0.30° N, 32.59° E) using optical counters. Data from Uganda and Ethiopia were used to compare the configuration applied to CHIMERE for Kenya with the two other countries (Table 2).

- Deleted: 3a, b, c
- Deleted: were provided by the ...ite located at Tom Mboya Street was usedin Nairobi
- Deleted: ..., 36.82°
- Deleted: the...site located inof...Nanyuki, Kenya (0.01° N, 37.07° E). B b
- Deleted: ..., 38.76° ...) and Uganda (0.30° ..., 32.59°

2.5 Statistical Parameters

Formatted: Font: Bold

In this work we use different statistical operators to evaluate the performance of WRF and CHIMERE models in reproducing the main surface weather parameters and hourly and daily concentrations of PM_{2.5} in different urban and rural environments. The statistical analysis both for WRF and for CHIMERE has been done calculating the statistics for each station individually and the averaging all station together. The calculation has been done on the original hourly values from observations and model outputs and consider hourly values from the model only if the corresponding hourly observation is present. The statistical parameters of Pearson's Coefficient (R, Eq. 2), index of agreement (IOA, Eq. 3), mean fractional bias (MFB, Eq. 4) and mean fractional error (MFE, Eq. 5) have been used for the calculations:

Formatted: Font: Bold

$$R = \frac{n(\sum_{i=1}^n M_i O_i) - (\sum_{i=1}^n M_i)(\sum_{i=1}^n O_i)}{\sqrt{[n \sum_{i=1}^n M_i^2 - (\sum_{i=1}^n M_i)^2][n \sum_{i=1}^n O_i^2 - (\sum_{i=1}^n O_i)^2]}} \quad \text{Eq. (2)}$$

Formatted: Font: 11 pt

Formatted: Left

Formatted

$$IOA = 1 - \frac{\sum_{i=1}^n (O_i - M_i)^2}{\sum_{i=1}^n (|M_i - \bar{O}| + |O_i - \bar{O}|)^2} \quad \text{Eq. (3)}$$

Formatted: English (United Kingdom)

Formatted: Font: 11 pt

Formatted: Left, Indent: Left: 0 cm

$$MFB = \frac{1}{n} \sum_{i=1}^n (M_i - O_i) / ((O_i + M_i) / 2) \quad \text{Eq. (4)}$$

Formatted

Formatted: Font: 11 pt

Formatted: Left

$$MFE = \frac{1}{n} \sum_{i=1}^n |M_i - O_i| / ((O_i + M_i) / 2) \quad \text{Eq. (5)}$$

Formatted

Formatted: Font: 11 pt

Formatted: Left

Formatted

MFB and MFE in particular, are metrics specifically used for the evaluation of numerical system for atmospheric chemistry and meteorology. They normalise the bias and the error for each model-observed pair by the average of the model and observation before taking the final average. The advantage of these metrics is that the maximum bias and errors are bounded, and that impact of outlier data points are minimised. Moreover, the metrics are symmetric giving equal weight, to concentrations simulated higher than observations and to those that are simulated lower than observations.

MFB and MFE have been expressed in terms of model performance "goals" and model performance "criteria" values according to the methodology proposed by Boylan and Russell (2006). The performance "goal" for the

434 modelling system is attested for $MFE \leq 50\%$ and $MFB \leq \pm 30\%$. In this range of the performance of the model in
 435 reproducing the correct magnitude of the concentrations can be considered good. A second larger range of values,
 436 called “criteria”, is attributed for $MFE \leq 75\%$ and $MFB \leq \pm 60\%$. Values inside this are corresponds to an average
 437 model performance. Finally, values with $MFE > 75\%$ and $-60\% > MFB > +60\%$ correspond to a poor
 438 representation by the model.

439 2.6 Model Resolution and Simulations design

441
 442 WRF and CHIMERE models run at spatial resolutions of 18×18 , 6×6 and 2×2 km for meteorology and at 6×6 and
 443 2×2 km for chemistry for the three domains of East Africa. The statistical analysis shown in the following sections
 444 though, describes the validation results for the three internal domains at a resolution of 2×2 km as these are the
 445 focus of the present work.

446
 447 Ground weather stations from the MIDAS database, included in the 2×2 km domains of all countries, were
 448 analysed individually, and shown as average of all stations. The time series and wind roses are relative to the
 449 closest stations from MIDAS database to each urban city centre of the three capital cities, namely Addis- Bole
 450 (n1 in Table 2), Kampala (n5 in Table 2) and Nairobi Airport (n7 in Table 2).

451
 452 Initially, the performance of CHIMERE was analysed for the domain of Kenya for which hourly concentrations
 453 of $PM_{2.5}$ were taken from two different sites (roadside and rural) from the field sampling campaign described by
 454 Pope et al., (2018). Secondly, the same configuration adopted for Kenya was used for Ethiopia and Uganda to test
 455 both the homogeneity of the emission rates on other urban conditions, and the configuration chosen for CHIMERE
 456 in different urban and environmental conditions. At this stage of the validation, a threshold limit of $25 \mu g m^{-3}$ for
 457 $PM_{2.5}$ per day provided by WHO (WHO, 2005) was used to quantify the number of exceedances observed and
 458 modelled by CHIMERE for the three cities.

459
 460 The validation process was hindered by the highly variable quantity and quality of available meteorological data.
 461 The majority of the weather observations are provided on a 3-hourly basis, with varying amounts of missing data.
 462 Despite this, the statistical evaluation of WRF has been performed comparing model and observations only when
 463 the latter were available. We recall that the objective of this work aims to test the performances of a modelling
 464 system for the simulation of air quality at high resolution for East Africa, updating and/or using the available input
 465 data available and assessing the possible adoption of these tools for air quality policy making at this extent of the
 466 data.

467 **3 Results and Discussion**

469 **3.1 Validation of the WRF simulations**

470
 471

Formatted: Font: Bold

Formatted: Font: Bold

Deleted: ¶
 ¶

Deleted: ¶

Deleted: The reliability of numerical simulation of meteorology and chemistry-transport processes need to be evaluated against observations to quantify the confidence of these systems. In the case of CTM in particular, this also to the capability to be used as tool for policy making, replicating scenarios and analysis purposes. While ozone modelling and evaluation has been fairly well developed over a number of decades, with the EPA (1991) criteria still used to evaluate the level of confidence of a CTM, for the PM evaluation the criteria used for the analysis of the performance are still evolving (Boylan and Russell, 2006).¶

¶
 In this work we use different statistical operators to evaluate the performance of WRF and CHIMERE models in reproducing the main surface weather parameters and hourly and daily concentrations of $PM_{2.5}$ in different urban and rural environments. The statistical parameters of Parson Coefficient (R) and index of agreement (IOA), mean fractional bias (MFB) and mean fractional error (MFE) have been used for the calculation. ¶

¶
 MFB and MFE in particular, are metric specifically used for the evaluation of numerical system for atmospheric chemistry and meteorology. They normalise the bias and the error for each model-observed pair by the average of the model and observation before taking the final average (Eq. 2 and 3). The advantage of these metrics is that the maximum bias and errors are bounded, and that impact of outlier data points are minimised. Moreover, the metrics are symmetric giving equal weight, to concentrations simulated higher than observations and to those that are simulated lower than observations. ¶

$$MFB = \frac{1}{N} \sum_{i=1}^N (C_m - C_o) / ((C_o + C_m) / 2)$$

Eq. (2)¶

$$MFE = \frac{1}{N} \sum_{i=1}^N |C_m - C_o| / ((C_o + C_m) / 2)$$

Eq. (3)¶

¶
 MFB and MFE have been expressed in terms of model performance “goals” and model performance “criteria” values according to the methodology proposed by Boylan and Russell (2006). The performance goal for the modelling system is attested for $MFE \leq 50\%$ and $MFB \leq \pm 30\%$. In this range of values (shown as green dashed lines in Figure 6) the performance of the model in reproducing the correct magnitude of the concentrations can be considered good. A second larger range of values, called criteria, is attributed for $MFE \leq 75\%$ and $MFB \leq \pm 60\%$. Values inside this are (shown as red dashed lines in Figure 6) corresponds to an average model performance. Finally values with $MFE > 75\%$ and $-60\% > MFB > +60\%$ a poor representation by the model. ¶

¶
 WRF and CHIMERE models run at spatial resolutions of 18×18 , 6×6 and 2×2 km for meteorology and at 6×6 and 2×2 km for chemistry for the three domains of East Africa. The statistical analysis shown in the following sections though, describes the validation results for the three internal domain(...

611 In order to assess the performance of WRF in simulating surface temperature, relative humidity wind speed and
612 direction, the model simulation outputs were compared with all the available ground weather station data available
613 for the period of analysis, 14th of February to 14th of March 2017. ▽

Deleted: Observations from the UK Met Office MIDAS database were available with variable frequency ranging from 1 to 6 hours.

615 3.1.1 Statistical evaluation of WRF performances

616
617 A statistical analysis, in terms of the mean fractional bias (MFB), mean fractional error (MFE), index of agreement
618 (IOA) and Pearson's coefficient (R), was carried out to compare modelled and observed values for the domain at
619 2×2 km resolution averaging the observed and modelled values on all the stations present on each domain (Table
620 3). We recall that the number and location of the stations is variable between the three domains (3 stations for
621 ETH2K and UGA2K and 5 stations for KEN2K).

622
623 The results of the statistical analysis show that WRF is capable of reproducing the mean levels of surface
624 temperature better for the domain of Ethiopia (ETH2K) and Uganda (UGA2K) with a mean underestimation over
625 the three domains of 1.4 and 1.5 °C, respectively, then for Kenya (KEN2K) where it shows an underestimation of
626 4.1 °C. The higher bias in surface temperature found on the average of all five stations of Kenya is though highly
627 driven by a particular poor representation of this variable at the observation point of Narok (n11 in Figure 2c)
628 where the bias between model and observations is 10.9 °C. A reason for this bias can be related by the location of
629 the station that is the one at highest altitude of all the Kenyan weather stations (2104 m a.g.l.). Narok is located
630 around 140 km west from Nairobi and the high bias in temperature should not have any effect on the levels of
631 temperature modelled in the capital of Kenya were the bias for the individual station of Nairobi (n7 in Figure 2c)
632 found was 1.3 °C.

Deleted: 3

Deleted: 3

633
634 Relative humidity is overestimated by WRF in KEN2K of 0.2 % and underestimated in ETH2K of 6.4 % and in
635 UGA2K of 7.5 % (Table 3). Wind Speed and directions for the three domains show respectively, the presence of
636 northern winds in UGA2K correctly captured by the model with a difference of around 4° in comparison with the
637 observations, an average eastern wind component in KEN2K partially reproduced by the model that allocates the
638 average wind directions on a more south-eastern component of wind with a difference of around 40.2° while in
639 ETH2K the average wind direction modelled and observed are closer with a difference of 4.2° on a south-eastern
640 component of prevailing wind. The observed and modelled wind speeds in UGA2K, KEN2K and ETH2K suggest
641 an overestimation by the model of 0.9, 0.8 and 0.2 m s⁻¹, respectively (Table 3).

Deleted: are in reasonable agreement with a

Deleted: model

642
643 The mean fractional error calculated in the three domains is inside the limit of the goal range both for surface
644 temperature and for relative humidity with values between 30 and 35 for the former and 11 and 27 for the latter
645 variable. On the other hand, the values of MFE for wind speed and directions are more variable according to the
646 domain. While MFE values for wind directions were found inside the criteria range for all domains, for wind
647 speed only KEN2K and ETH2K are in this range, while the wind speed in UGA2K was found outside the
648 acceptability range of model performance (Table 3).

657 The same analysis done taking in account the mean fractional bias shows values in the goal range for surface
 658 temperature for the three domains, overestimated by the model for UGA2K (0.17) and underestimated for ETH
 659 2K (-5.38) and KEN2K (-24.25). Same behaviour was found also for the relative humidity that seems
 660 underestimated in the three domains but with MFB values inside the goal criteria. Finally, wind speed and
 661 directions are found in the goal range of MFB only for ETH2K while KEN2K shows values of both variables in
 662 the criteria range and UGA2K shows wind direction in the criteria range but wind speed outside the acceptability
 663 range of model performance (Table 3).

665 **Table 3:** Statistical analysis of relative humidity, surface temperature, wind speed and directions averaged on all the available
 666 weather stations for the second nested domains UGA2K, KEN2K and ETH2K at 2×2 km of resolution. Mean observed and
 667 modelled values, Pearson's Coefficient (R), index of agreement (IOA), mean fractional bias (MFB) and error (MFE) have
 668 been calculated.

	Relative Humidity (%)			Temperature (°C)		
	UGA2K	KEN2K	ETH2K	UGA2K	KEN2K	ETH2K
Observations Mean	68.2	63.1	51.3	24.5	23.2	22.7
Model Mean	60.7	63.3	44.9	23.0	19.1	21.3
MFB	-21.52	-21.36	-33.02	0.17	-24.25	-5.38
MFE	30.08	32.25	35.56	12.50	27.94	11.34
IOA	0.44	0.44	0.47	0.43	0.31	0.53
R	0.3	0.4	0.7	0.3	0.5	0.6
	Wind Direction (degrees)			Wind Speed (m s ⁻¹)		
	UGA2K	KEN2K	ETH2K	UGA2K	KEN2K	ETH2K
Observations Mean	6.8	91.5	104.0	2.5	2.7	3.5
Model Mean	2.8	131.7	99.8	3.4	3.5	3.7
MFB	32.02	-30.57	-9.94	91.25	36.83	18.89
MFE	62.01	70.55	60.18	94.59	54.35	50.63
IOA	0.39	0.40	0.46	0.26	0.41	0.31
R	0.3	0.2	0.2	0.1	0.5	0.4

669 The calculated Pearson's coefficient (R) shows the capability of the model in reproducing the minimum and
 670 maximum peaks of different variable values. The R values were found varying between 0.1 and 0.7 for the three
 671 domains. The reproduction of the maximum and minimum values of relative humidity is better in ETH2K, where
 672 R value was found approximately 0.7, while the lowest R values occurred in UGA2K (0.3). A similar trend was
 673 found also in the description of the surface temperature, with maximum and minimum better reproduced in ETH2K
 674 (0.6), followed by KEN2K (0.5) and UGA2K (0.3). For wind speed, the highest R coefficient value was for
 675 KEN2K (0.5) and the lowest for UGA2K (0.1) while for wind directions, the highest R value found was for
 676 UGA2K (0.3) with values of approximately 0.2 for the other two domains (Table 3).

677 Finally, the evaluation of the index of agreement (IOA) shows values for surface temperature between 0.31
 678 (KEN2K) and 0.53 (ETH2K) and values between 0.44 and 0.47 for relative humidity in the three domains. For
 679 wind speed and directions, the IOA varies between 0.39 (UGA2K) and 0.46 (ETH2K) for the former and between
 680 0.26 (UGA2K) and 0.41 (KEN2K) for the latter. The comparison of the Index of Agreement between the three
 681 domains suggests that the model performance is higher in reproducing drier areas corresponding to ETH2K and
 682 KEN2K in comparison with the UGA2K where the influence of the Lake Victoria seems to impact the overall
 683
 684

Deleted: (Obs. Mean, Model Mean)

Deleted: .

Formatted Table

Deleted: .

Deleted: .

Deleted: 67

Deleted: 49

Deleted: ¶

All the relative humidity and surface temperature values of MFE were found in the performance goal range for the three domains: UGA2K (30.08 and 12.50, respectively) KEN2K (32.25 and 27.94) and ETH2K (35.56 and 11.34). The same evaluation done on wind direction and speed shows for the former MFE values inside the criteria performance range (62.01 for UGA2K, 70.55 for KEN2K and 60.18 for ETH2K) but for wind speed only KEN2K and ETH2K are in the criteria range (54.35 and 50.63, respectively) while wind speed in UGA2K is found outside the range of acceptability of the metric (94.59) (Table 3). The MFB analysis shows that surface temperature is inside the range of performance goal in all three domains with UGA2K (0.17) showing the best performance in reproducing the variable. The MFB values inside the goal criteria were found for the domain of UGA2K and KEN2K also for relative humidity (-21.52 and -21.36) while for ETH2K the value of MFB was found in the criteria range (-33.02). The ETH2K is the only domain that shows MFB in the goal range for the evaluation of wind direction (-9.94) and speed (18.89). The domain of Kenya (KEN2K) shows both values inside the criteria range with -30.57 for wind direction and 36.83 for wind speed. Finally, UGA2K shows wind direction inside the criteria range (32.02) but wind speed outside the range of acceptability of this metric (91.25) (Table 3). ¶

Deleted: varying agreement

Deleted: between the model and observations with values

Deleted: The highest

Deleted: for relative humidity of approximately

Deleted: was obtained for ETH2K

Deleted: Highest values of

Deleted: R for surface temperature were found

Deleted: s

Deleted: are

Deleted: for

Deleted: the

Deleted: for

729 [statistical analysis. More variable is the performance of WRF in reproducing the general conditions of wind speed](#)
730 [and directions between the three domains.](#)

731

732 3.1.2 Hourly variation of Temperature and Relative humidity

733

734 The three [Met Office](#) stations providing weather observations closest to the urban areas of the Addis Ababa,
735 Kampala and Nairobi have been analysed individually in form of hourly time series of surface temperature and
736 relative humidity and wind roses for wind speed and directions.

737

738 The hourly surface temperature and relative humidity are shown in Figure 4 for the three ground weather stations
739 closest to the centre of the three cities: Addis-Bole (n1 in Figure [2a](#)), Kampala Station (n5 in Figure [2b](#)) and
740 Nairobi (n7 in Figure [2c](#)).

741

742 The temperature range observed at the three stations was between 9 and 27° C for the Addis-Bole Station, 16 and
743 31° C for Kampala and 16 and 33° C for Nairobi. By inspection of Figure 4, it can be seen that the WRF model
744 is able to reproduce the main diurnal cycle of variation of temperature and relative humidity for the three ground
745 weather stations. Surface temperature peaks are slightly underestimated by the model for the three stations with a
746 small mean bias at the three stations between -0.06 and -0.1° C. The highest agreement between the model and
747 observation is for Kampala while the model tends to underestimate the diurnal peaks of surface temperature almost
748 systematically for Addis-Bole and Nairobi stations.

749

750 [The mean relative humidity observed at the three stations shows different ranges of excursion from the model](#)
751 [predictions depending on the characteristics of the environment. The station of Addis-Bole shows the higher](#)
752 [variation from 15 to 98 %, Nairobi station from 17 to 98 % and Kampala from 19 to 99 %. From Figure 4, it may](#)
753 [be seen that relative humidity variation over time is correctly captured by WRF for the Nairobi and Addis-Bole](#)
754 [stations. Despite this both the diurnal peaks and night lowest values seems to be not correctly reproduced by the](#)
755 [model that tends to overestimate the formers and underestimate the latter with a bias between -0.1 and 0.004 %.](#)

756

757 [However, WRF appears systematically to underestimate the relative humidity for the Kampala station showing a](#)
758 [mean negative bias. Different reasons could affect the underestimation of the relative humidity at this station. The](#)
759 [sensitivity of WRF model to the land use data \(Teklay et al., 2019\) connected with the proximity of Kampala to](#)
760 [Lake Victoria, which is a massive inland body of water \(surface area 68,800 km²\) could influence the local](#)
761 [variation of relative humidity in ways which are not well reproduced by the model. The influence of Lake Victoria](#)
762 [and of the Kampala's complex topography on measurements of relative humidity was previously highlighted by](#)
763 [Singh et al. \(2020\) in relation to monthly visibility connected with PM levels. It has to be noted that relative](#)
764 [humidity was calculated from surface temperature and dew point values following Alduchov O. \(1996\) and not](#)
765 [directly sampled. A better agreement in the simulation of relative humidity from WRF can be found in the station](#)
766 [of Entebbe \(n4 in Figure \[2b\]\(#\)\) where the mean normalized bias shows a small underestimation of 0.04 %.](#)

767

Deleted: MIDAS

Deleted: 3

Deleted: 3

Deleted: 3

Deleted:

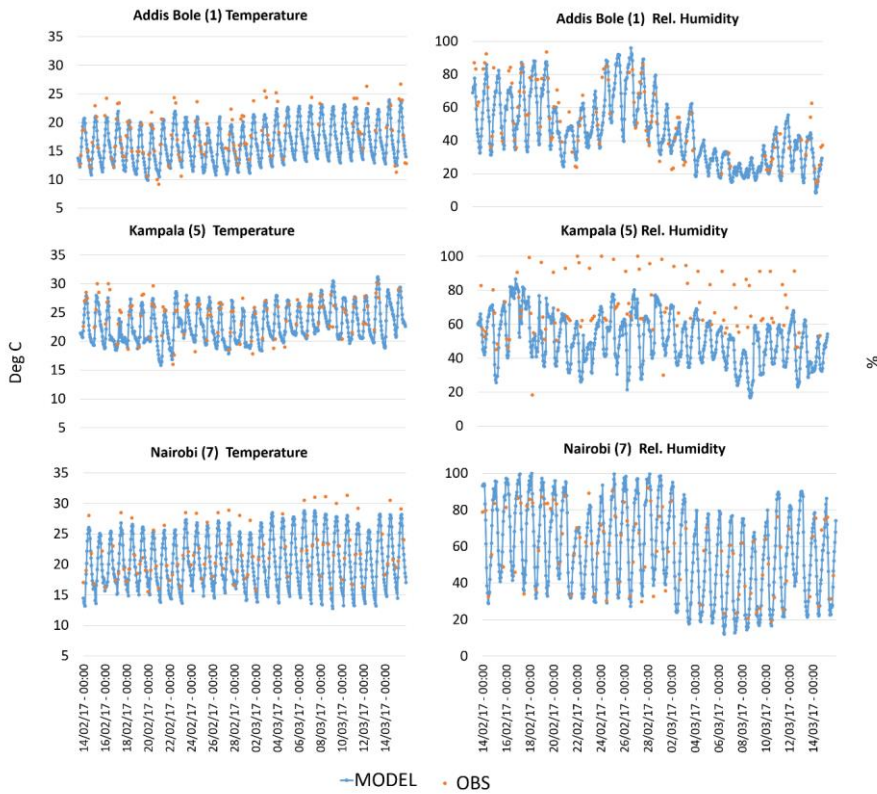
Deleted: s

Deleted: are

Deleted: RH

Deleted: Noting

Deleted: 3



778
779 **Figure 4:** Hourly time series of surface temperature (left column) and relative humidity (right column) for the closest ground
780 weather stations to the urban centres of the cities of Addis Ababa (station 1 in Figure 2a), Kampala (station 5 in Figure 2b)
781 and Nairobi (station 7 in Figure 2c). Comparison between modelled values (blue lines) obtained from the 2x2km domains
782 and hourly observations (orange spots) from *Met Office MIDAS* database.
783

784 [Wind speed and directions from the urban stations of Addis Bole \(n1 in Figure 2a\), Kampala Station \(n5 in Figure](#)
785 [2b\) and Nairobi \(n7 in Figure 2c\) are shown in Figure 5 in the form of wind roses. WRF can reproduce the average](#)
786 [wind directions in close agreement with the observed data for the analysed period for Nairobi showing the](#)
787 [predominance presence of North-North-Eastern winds with high speed \(> 4.0 m s⁻¹\). Wind speed observations](#)
788 [from the ground weather station of Kampala also suggest a strong southern wind component \(> 4.0 m s⁻¹\) while](#)
789 [the model seems to reproduce a similar magnitude of the wind speed but on a larger range of directions ranging](#)
790 [from the South-South-East direction to South-South-West. For Addis Ababa, WRF seems able to capture and](#)
791 [reproduce the main wind directions observed for the simulated period, e.g., Eastern and North-Eastern winds.](#)
792 [Despite this, slower winds between 0.2 and 2.0 m s⁻¹ with a strong North-Northeast component do not seem to be](#)
793 [replicated by the model for the station located inside the capital of Ethiopia.](#)

Deleted: 3

Deleted: 3

Deleted: 3

Deleted: MIDAS

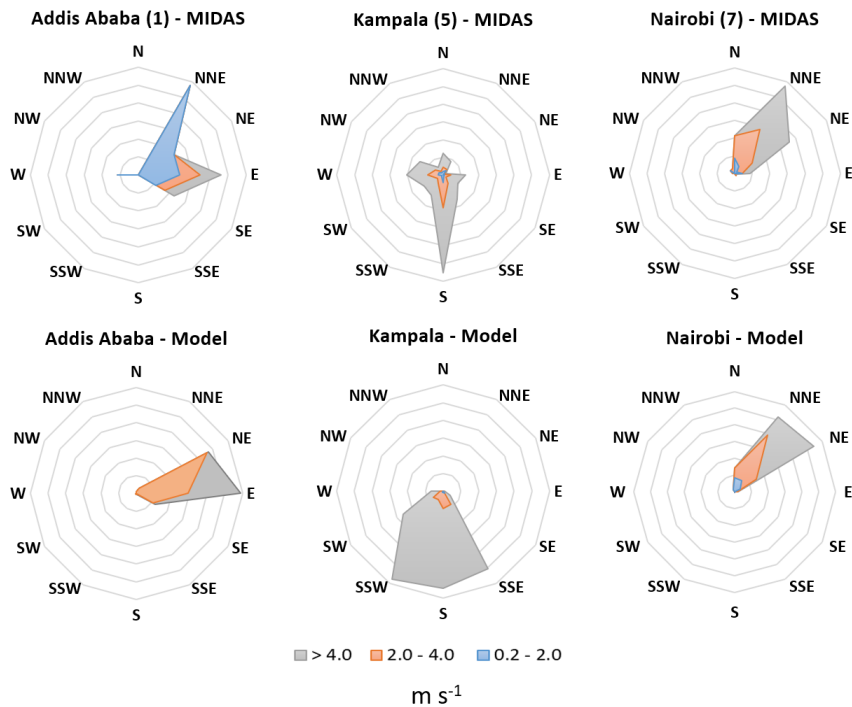
Deleted: -

Deleted: 3

Deleted: 3

Deleted: 3

Deleted: Moreover, the model replicates the wind directions for Nairobi with higher agreement in comparison to Addis Ababa and Kampala.



805
 806 **Figure 5:** Averaged wind roses for the whole analysed period (14th of February to 14th of March 2017) from the closest ground
 807 weather stations to the urban centres of Nairobi (n7 in Figure 2c), Kampala (n5 in Figure 2b) and Addis Ababa (n1 in Figure
 808 2a) (MIDAS, top) and from WRF simulation outputs (Model, bottom).

809
 810 The lower agreement in the reproduction of the wind speed and direction in Addis Bole and Kampala stations can
 811 be connected to the particular locations of both stations. The difference in the location of the observations can, in
 812 fact, influence rapid changes in directions and speed locally recorded and not reproduced by the model. In the
 813 case of Kampala, the airport “Entebbe” is located near the coast of the Lake Victoria where the local conditions
 814 of wind are more susceptible of variation and can be erroneously reproduced by the model. In the case of Addis
 815 Bole, the only station settled in the urban area, the urban topography and possible canyon effects of the wind can
 816 be not well captured by the model that reproduces a more constant range of wind speed and directions not
 817 accounting for quick variations at low speed observed at the station.

818
 819 The results obtained from the validation of the meteorological simulations performed over East African domains
 820 using WRF show that the model is on average able to reproduce all four variables taken in account close to the
 821 observed data in the 2x2 km domains with variable agreement between the three cities. The highest agreement in
 822 the weather analysis has been found for surface temperature with similar biases to Kerandi et al. (2017) and

- Deleted: 3
- Deleted: 3
- Deleted: 3
- Deleted: MIDAS
- Deleted: that the station of Addis-Bole is the only one settled inside an urban area, while the stations of Kampala and Nairobi are settled in the respective airports located in peri-urban areas.
- Deleted: have an
- Deleted: on
- Deleted: the
- Deleted: in the observations
- Deleted: These rapid changes given by the open spaces (airport), or...the the
- Deleted: the
- Deleted: of urban areas cannot
- Deleted: WRF that take in account of a differentiation of the land use between urban and not urban areas

842 [relative humidity similar to Pohl et al. \(2011\), which is sufficiently accurate to be able to use these values for the](#)
843 [physical calculations done by the chemistry transport model.](#)

844
845 [Nevertheless, the more detailed analysis of the urban weather stations revealed discrepancies in the reproduction](#)
846 [of relative humidity and wind direction for the station of Kampala \(UGA2K\) that could affect the deposition,](#)
847 [removal and transport processes simulated by CHIMERE and will be object of future investigation to further](#)
848 [improve the meteorological performance of WRF. Even if the bias found for some variable in the calculation of](#)
849 [the averaged statistics over all stations was high, the individual weather stations close to the urban areas of interest](#)
850 [showed smaller bias and levels of MFB and MFE inside the goal or criteria range of performance and therefore](#)
851 [considered acceptable for simulations.](#)

852 853 **3.2 Validation of CHIMERE simulations**

854
855 [The CHIMERE validation has been focused on the hourly levels of PM_{2.5} modelled at the two observation sites](#)
856 [for the domain KEN2K, representative of a roadside site and a rural background site. Also, from the urban](#)
857 [background observational sites of the U.S. Embassies of Kampala \(UGA2K\) and Addis Ababa \(ETH2K\). The](#)
858 [performance of CHIMERE was analysed also in terms of mean fractional error \(MFE\), mean fractional bias](#)
859 [\(MFB\) and Pearson's coefficient \(R\) against the different level of average concentrations of PM_{2.5} in the four](#)
860 [observation points to evaluate the response of the model in reproducing low and high levels of hourly](#)
861 [concentrations in comparison with observed values.](#)

862
863 [The validation of CHIMERE was done for the domains at highest resolution \(2×2 km\) despite the availability of](#)
864 [emissions at a similar spatial resolution. The reason of this choice is motivated by the necessity to validate the](#)
865 [reliability of the model against observation data from particular locations in different backgrounds. In order to](#)
866 [better configure the model to represent the different urban and rural environments it is necessary to take in account](#)
867 [the uncertainties of a model representation against an observation point. One cause of uncertainty when comparing](#)
868 [modelling outputs with observations is the difference between a point measurement and a volumetric grid cell](#)
869 [averaged modelled concentration \(Seinfeld, 2016\). On one hand, the extent of a measurement point, in fact,](#)
870 [represents only the extent of the nearby points or an average concentration in a specified area. On the other hand,](#)
871 [a surface level modelling grid typically has highest resolution of 1 km with a vertical height of between 20 and](#)
872 [40 m and the concentration represented by the model is the average over the entire grid cell.](#)

873
874 [In the particular case of the domains of East Africa, CHIMERE simulates at coarse resolution e.g., the 6×6 km,](#)
875 [values of concentration representative of an average of 36 km², difficult to be compared with observations taken](#)
876 [in a particular point. Increasing the spatial resolution and bringing it to 2×2 km the average value inside each grid](#)
877 [cell will be representative of a smaller area such as 4 km² whose average value can be closer compared with an](#)
878 [individual observation point.](#)

879 880 *3.2.1 Statistical evaluation of model performances*

881

Deleted: However, for the purposes of the present work the range of bias found for the meteorological variables can be considered acceptable.

885 The absolute bias between mean observed and modelled concentrations of PM_{2.5} shows an overestimation of the
886 model for the domain KEN2K by between 0.01 and 3.7 µg m⁻³ for Nanyuki and Nairobi, respectively, and for
887 Addis Ababa (0.6 µg m⁻³). On the contrary, the model underestimates PM_{2.5} for the domain UGA2K (Kampala)
888 by 7.2 µg m⁻³ (Table 4).

Deleted: 6

889 The mean fractional bias (MFB) and error (MFE) for the two Kenyan observation points were found in both cases
890 inside the goal performance criteria with MFE < 50% and MFB < ± 30% both in Nairobi (roadside site) and in
891 Nanyuki (rural site). The hourly MFB and MFE were 4.88 and 25.39 for Nairobi and 3.36 and 8.33 for Nanyuki
892 while 0.1 and 1.99 for Nairobi and 1.08 and 4.73 for Nanyuki were the respective values found for the daily
893 analysis.

894
895
896 The MFB and MFE analysis for the urban background site in Addis Ababa showed values inside the range of the
897 goal criteria both for the hourly (2.93 and 29.99 for MFB and MFE) and for daily analysis (8.23 and 2.86). Finally,
898 in the urban background site of Kampala the MFB were found inside the goal criteria both for daily (-11.28) and
899 hourly (-7.60) analysis, while for the MFE the hourly analysis showed a value in the range of the criteria range
900 (32.99) but daily MFE in the goal performance range (22.06) (Table 4).

901
902 The highest Pearson's coefficients (R) were found in Nanyuki with hourly and daily values of between 0.91 and
903 0.93. The roadside site of Tom Mboya Street in Nairobi had R values of between 0.35 and 0.38 while the urban
904 background sites of Addis Ababa and Kampala had a lower agreement an hourly level (R values were between
905 0.10 and 0.29, respectively) than at a daily level (R values of between 0.42 and 0.30, respectively).

906
907 In general, the statistical analysis demonstrates that the model can reproduce the daily pattern of the hourly
908 changes in concentrations for the two pollutants both in the three urban/roadside sites and in the rural site
909 considered. The low R coefficient values obtained for the urban domains at the hourly level suggests that sources
910 of anthropogenic emissions affecting urban air quality are still missing from the current emission inventory.
911 Further work will be focused on the improvement of the magnitude of the emissions to better match the observed
912 levels of concentrations of particulate matter at the urban level. Despite this and considering the daily average
913 concentrations in the urban sites, the R coefficients were found to be between 30 and 42 % suggesting that
914 CHIMERE better reproduces the concentrations of PM_{2.5} using daily than hourly values.

Deleted: averaging

915
916 The performance of CHIMERE varies between the domains of Kenya, Uganda, and Ethiopia. The performance
917 of the model has been optimised during the validation for the simulation of hourly concentrations of PM_{2.5} in
918 Kenya and the same configuration applied to the domain of Uganda and Ethiopia to compare the reliability of the
919 model. The difference in performance can be connected to different reasons: In first place, the difference in the
920 sampling methods used for the two sites in Kenya against the measurements taken in the U.S. Embassies of
921 Kampala and Addis Ababa. Secondly, another element of differentiation can be connected to the location of the
922 observation sites in the cases of the U.S. Embassies and/or the possible influence of local sources not accounted
923 in the emission inventories.

Deleted: ¶

924

928 **Table 4:** Hourly and daily statistical evaluation of CHIMERE model performance for the cities of Nairobi against ASAP
 929 observed data and against U.S. Embassies data for the cities of Addis Ababa and Kampala.

ASAP Observations	NAIROBI PM _{2.5} (µg m ⁻³) roadside		NANYUKI PM _{2.5} (µg m ⁻³) rural	
	DAILY	HOURLY	DAILY	HOURLY
Model Mean	58.3	58.3	3.24	3.24
Observations Mean	54.6	54.6	3.23	3.23
MFB	0.1	4.88	1.08	3.36
MFE	1.99	25.39	4.73	8.33
R	0.38	0.35	0.93	0.91
U.S. EMBASSY Observations	ADDIS ABABA – PM _{2.5} (µg m ⁻³) urban		KAMPALA – PM _{2.5} (µg m ⁻³) urban	
	DAILY	HOURLY	DAILY	HOURLY
Model Mean	18.7	18.7	36.2	36.2
Observations Mean	18.1	18.1	43.4	43.4
MFB	8.23	2.93	-11.28	-7.60
MFE	2.86	29.99	22.06	32.99
R	0.42	0.10	0.30	0.29

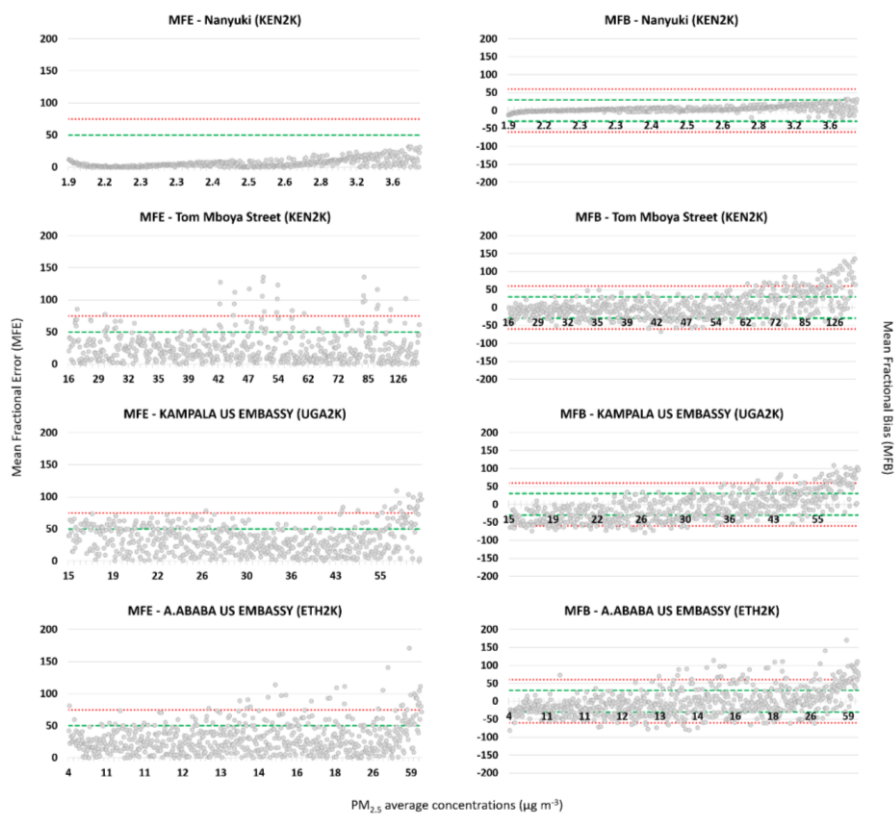
930
 931 Finally, the site of Nanyuki is the location where the agreement between model and observations is highest. This
 932 site was chosen by Pope et al. (2018) as rural spot in a location of minimum local air pollution useful to calculate
 933 the net urban increment subtracting the rural background concentrations of Nanyuki from the urban concentrations
 934 in Nairobi. It is therefore intended by their work that the average concentrations in that site were really low. The
 935 model is able to reproduce this low level of contamination close to the reality and to reproduce also peaks of
 936 contamination in particular days of February probably generated elsewhere (see Section 3.2.2).

937
 938 The MFB and MFE analysis have been conducted also at hourly level comparing modelling outputs and
 939 observations from all six sites in relation to the magnitude of hourly concentrations (Figure 6).

940
 941 There are some MFB values outside the criteria range for PM_{2.5} for the urban sites of Addis Ababa and Kampala
 942 and for the roadside site of Tom Mboya Street in Nairobi. In terms of the upper limit (MFB > 60 %) these values
 943 tend to be concentrated between 60 and 130 µg m⁻³ for Tom Mboya Street, 40 and 55 µg m⁻³ for Kampala and
 944 between 13 and 59 µg m⁻³ for Addis Ababa (Figure 6). A much smaller number of MFB values for the Addis
 945 Ababa and Kampala sites are less than the lower criteria limit and these tend to be for lower concentrations
 946 between 10 and 26 µg m⁻³.

947
 948 MFE values outside the ranges of criteria are between 42-55 and 80-130 µg m⁻³ for Tom Mboya Street, 43 and 60
 949 µg m⁻³ for Kampala and 13 and 59 µg m⁻³ for Addis Ababa (Figure 6). The latter two sites present a more variability
 950 of MFB and MFE in comparison with the two sites of Kenya where is visible a common positive bias of the model
 951 in reproducing the highest concentration levels. The reliability of the model is therefore higher for the domain of
 952 Kenya, both for a rural and for a roadside site than for the two urban background sites in Uganda and Ethiopia.

- Deleted: /
- Deleted: /
- Formatted: Superscript
- Formatted: Superscript
- Formatted Table
- Deleted: OBS
- Deleted: Mean MOD
- Formatted: Left
- Deleted: Mean OBS
- Formatted: Left
- Deleted: DDIS A.
- Deleted: /
- Formatted: Superscript
- Formatted: Spanish (Chile)
- Deleted: /
- Deleted: ³
- Formatted: Spanish (Chile)
- Deleted: OBS
- Formatted: Left
- Deleted: Mean MOD
- Deleted: Mean OBS
- Formatted: Left
- Formatted: Left
- Formatted: Left
- Formatted: Left
- Deleted: ¶
- Deleted: r
- Deleted: has



969
 970 **Figure 6:** Hourly mean fractional bias (MFB) and mean fractional error (MFE) values calculated for the locations of Tom
 971 Mboya Street and Nanyuki (KEN2K), Kampala U_S Embassy (UGA2K) and Addis Ababa U_S Embassy (ETH2K) for the
 972 analysed period against hourly concentrations of PM_{2.5}. The green lines represent the MFB range $\pm 30\%$ and the MFE limit
 973 of 50 % for which the model performance can be considered reliable, the red lines represent the MFB range $\pm 60\%$ and the MFE
 974 limit of 75 % for which model performance can be increased by diagnostic analysis on the chemical precursors of PM_{2.5}.
 975

Deleted: % for

976 The overall performance of the model against different levels of concentrations is summarised in Table 5. The
 977 PM_{2.5} reproduced at the two sites in KEN2K shows a higher percentage of values within the MFB and MFE
 978 performance goals for the rural site of Nanyuki, than for Tom Mboya Street. *e.g.*, 97 % compared to 69 % and 99
 979 % compared to 88 % for the MFB and MFE measures respectively. For the criteria measure, the corresponding
 980 percentages are 2 % vs. 22 % and 1 vs. 7 % (Table 5).

981
 982 The percentages for the urban sites of Kampala and Addis Ababa show a lower agreement between the model and
 983 observations. For the former 48 % of the values according to the MFB measure are within the goal range, 37 %
 984 are within the criteria range and 15 % are outside. For the latter, according to the MFB criteria, 57 % of the values
 985 are inside the goal range, 30 % of values are within the criteria range and 13 % are outside. In terms of the MFE
 986 measure, 74 % and 80 % of values for the two cities are within the goal range, 16 % and 11 % within the criteria
 987 range and 10 % and 9 % outside respectively (Table 5).

989
990
991
992

Table 5: Hourly mean fractional bias (MFB) and error (MFE) percentage of points inside the goal limit (GOAL), inside the diagnostic range (CRITERIA) and outside the reliability criteria (OUT) from model outputs extracted from the four analysed locations.

Location	MFB			MFE		
	GOAL (%)	CRITERIA (%)	OUT (%)	GOAL (%)	CRITERIA (%)	OUT (%)
Tom Mboya Street (KEN2K)	69	22	9	88	7	5
Nanyuki (KEN2K)	97	2	1	99	1	0
Kampala (UGA2K)	48	37	15	74	16	10
A. Ababa (ETH2K)	57	30	13	80	11	9

Formatted Table

Deleted: City

Deleted: .

993

994 According to the methodology proposed by (Boylan and Russel, 2006) the performance of a modelling system is
995 fairly good for PM_{2.5} representation if about the 50 % of the points are within the goal range and a large majority
996 are within the criteria range. From the analysis of the four sampling sites the values of MFB inside both the goal
997 and range for Tom Mboya Street are 69 %, 97 % for Nanyuki and 57 % for Addis Ababa and only for Kampala
998 are 48 %. Similarly, for the MFE measure, 99 % for Nanyuki, 88 % for Tom Mboya Street, 80 % for Addis Ababa
999 and 74 % for Kampala are inside both the goal range. The demonstrates that the performance of the model can be
1000 considered to be satisfactory (Table 5).

1001

1002 Finally, the reason for the presence in the Addis Ababa and Kampala simulations of values outside the criteria
1003 range both at high and at low concentrations of PM_{2.5} can be connected to the representation of the original PM
1004 emissions in the combined inventory. It is possible that CHIMERE is not able to correctly reproduce all the
1005 chemical processes involved in the secondary formation of inorganic and organic individual components of PM_{2.5}
1006 with the extent of the present input data. Moreover, the possible misrepresentation of local emission sources not
1007 reproduced in DICE-EDGAR can also affect the performance of the model. Finally, the different location of the
1008 urban background observation sites and the sampling techniques for PM observation can also have a key role in
1009 the correct detection of the concentrations.

1010

3.2.2 Hourly variation of PM_{2.5} in urban and rural sites of Kenya

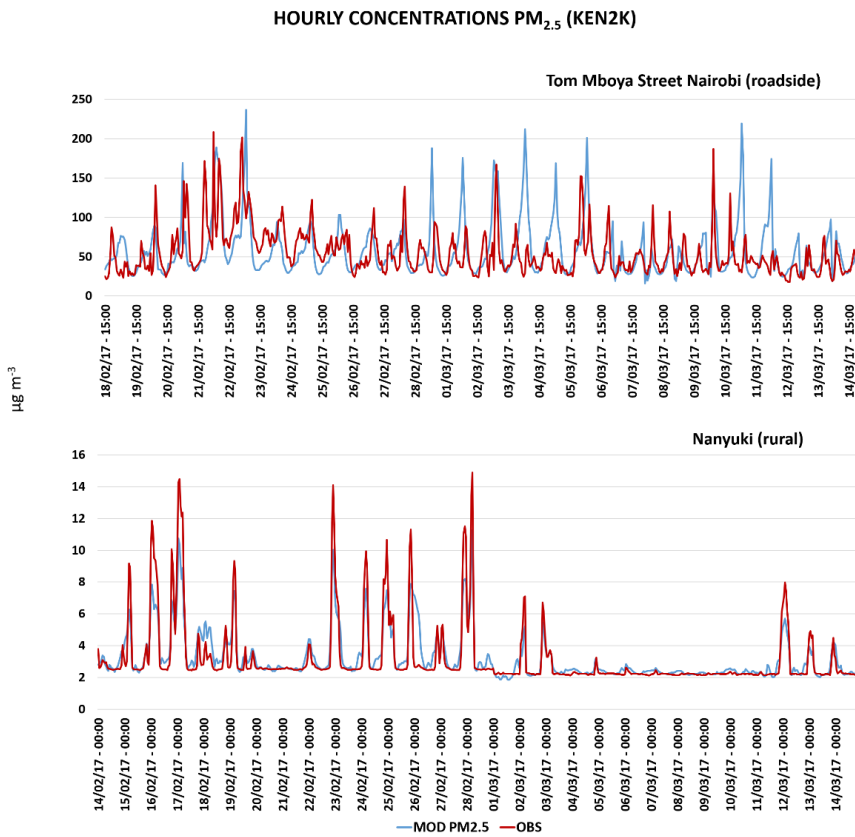
Deleted: 3

1012

1013 Hourly modelled variation of PM_{2.5} levels obtained by CHIMERE compared with observations are shown for the
1014 urban sampling site of Tom Mboya Street in Nairobi and for the rural site of Nanyuki (Figure 2c).

Deleted: 3

1015



1020

1021 **Figure 7:** Hourly time series for PM_{2.5} from the roadside of Tom Mboya Street (top) and from the rural site of Nanyuki (bottom)
 1022 from modelled output from CHIMERE model (blue line) and observed values from Pope et al. (2018) (red line) for the analysed
 1023 period. The simulation started on the 14th of February. For the Tom Mboya Street site only the period of time between the 18th
 1024 of February and the 14th of March when observations were available has been shown in the timeseries.
 1025

1026 By inspection of Figure 7 it can be seen that CHIMERE is able, in general, to reproduce the daily variation of
 1027 PM_{2.5} across the simulated period at both sites. The magnitude of the emissions adopted seems to be suitable both
 1028 for the roadside area of Tom Mboya Street and for the rural background site of Nanyuki, with higher agreement
 1029 shown by the latter. CHIMERE captures only part of the daily peak observed in Tom Mboya Street with
 1030 comparable magnitude but misrepresents some peaks. In particular it models higher hourly peaks than those
 1031 observed as previously mentioned in the MFB and MFE analysis.
 1032

1033 The misrepresentation of some high peaks in Tom Mboya Street is possibly due to a number of different reasons.
 1034 Firstly, is important to recall that the point measurements and relative observed concentrations are representative
 1035 of a smaller portion of space in comparison with grid-cell concentrations modelled. In this particular case the
 1036 comparison is between a roadside site subjected to possible additional local sources of PM_{2.5} not accounted for in

1037 the emissions and not correctly reproduced by CHIMERE. On the other hand, a few of the modelled peaks were
1038 overestimated. This can be addressed by improved temporal description of the emissions and in their magnitude
1039 in comparison to the reality. As mentioned previously, the anthropogenic emissions used in this work were the
1040 most up-to-date available at the time and that there is inevitably some difference between the measured data due
1041 to the difference in time between the inventories and the measurements. Despite this, there is reasonable agreement
1042 between model outputs and observed concentrations for the majority of the analysed period highlighting the
1043 reliability of CHIMERE in describing the hourly concentrations trends for a roadside site with expected high
1044 levels of PM_{2.5} contamination.

1045
1046 Similarly, in the rural site of Nanyuki, the model seems to correctly reproduce the hourly variation of the
1047 concentrations during the whole period, underestimating the maximum peaks at the beginning of February and in
1048 the last four days of simulation in March. (Figure 7). The site shows different magnitude in the concentrations of
1049 PM_{2.5} when comparing the February and March periods. While between the 4th and the 10th of March hourly
1050 concentrations are around 3-4 µg m⁻³, previously and subsequently to this period of time, the concentrations of
1051 PM_{2.5} are more than two times higher. This behaviour is visible both in the observations from the site (red line in
1052 Figure 7, bottom) and from the model outputs obtained using CHIMERE (blue line in Figure 7, bottom).

1053
1054 The site of Nanyuki was chosen by Pope et al. (2018) as rural spot in a location of minimum local air pollution
1055 influence. Data from Nanyuki was used for the calculation of the net urban increment subtracting the rural
1056 background concentrations of Nanyuki from the urban concentrations in Nairobi. The average concentrations
1057 around 3-4 µg m⁻³ in the period between the 4th and the 10th are, on one hand, levels of the rural background in
1058 absence of any external influence from meteorological parameters and in absence of local sources.

1059
1060 On the other hand, the presence of higher hourly peaks in before and after the 4th to 10th can be linked to different
1061 reasons: the presence of local emission sources contributing to the peaks or the dispersion of polluted air masses
1062 from elsewhere towards the site of Nanyuki. It is important to observe that model and observations seems to agree
1063 particularly well in the description of the difference in magnitude between the different time periods excluding
1064 the possibility that the observed values can be influenced by local emission sources not accounted in the emission
1065 inventory. It seems more likely that those concentration levels are transported to Nanyuki from neighbouring areas
1066 with higher levels of PM_{2.5} contamination. To investigate this possible role of PM_{2.5} dispersion towards Nanyuki,
1067 we consider the closest MIDAS weather station to the sampling area of Nanyuki, in the town of Nyeri (0.43°S,
1068 36.95°E altitude 1916 m a.g.l.) (n10 in Figure 2). Nyeri is only 60 km from the Nanyuki site and is situated
1069 between Mount Kenya (0.10°S, 37.30°E, altitude 4341 m a.g.l.) to the west and the Aberdare Range (0.46°S,
1070 36.69°E, altitude 3441 m a.g.l.).

1071
1072 The daily average concentrations observed in the sampling site of Nanyuki have been compared with the daily
1073 mean values of wind speed and directions observed at the MIDAS station of Nyeri and with the daily mean values
1074 of wind speed and directions modelled by WRF in Nanyuki (Figure 8). The period between the 4th and the 10th of
1075 March, when the daily average concentrations of PM_{2.5} observed in Nanyuki were around 2.2 µg m⁻³ corresponds
1076 to higher wind speed conditions (between 4 and 5 m s⁻¹) mainly coming from North-Est (around 60 degrees). In

Deleted: 0

Formatted: Superscript

Formatted: Superscript

Formatted: Superscript

Formatted: Superscript

Formatted: Superscript

Deleted: ¶

¶
One of the few possible reasons for this different behaviour may be weather conditions of wind speed and wind directions during February and March in th area.

Formatted: Subscript

Formatted: Subscript

Deleted: T

Deleted: is

Deleted: 3

1086 the same period, at Nyeri the modelled wind speed was low (between 1 and 2.5 m s⁻¹) and mainly with a westerly
 1087 component (between 220 and 300 degrees).
 1088

1089 In the periods of higher average daily concentrations of PM_{2.5} between the 15th and the 19th and between 22nd and
 1090 the 28th of February 2017, both in Nyeri (using observations) and in Nanyuki (using model outputs) the component
 1091 of wind directions seems to be consistent in reproducing southern winds (between 120 and 190 degrees) with wind
 1092 speeds between 1.5 and 2.5 m s⁻¹ in the first period and between 2 and 3 m s⁻¹ in the second period.

1094 [The correspondence between the wind speed and directions in particular time periods and the vicinity of the towns](#)
 1095 [could suggest the potential dispersion of pollutants from the southern area where the hotspot of Nyeri is located](#)
 1096 [upwind in the northern area of Nanyuki \(downwind\) in accordance with the wind fluxes from south to north from](#)
 1097 [Nyeri from the observations and also from WRF outputs extracted from the Nanyuki location. The flux could also](#)
 1098 [be driven by the location of Nyeri sited at the entrance of a basin between two mountain ranges. On the other](#)
 1099 [hand, in the period of low concentrations between the 4th and the 10th of March north-eastern winds \(around 60](#)
 1100 [degrees\) blow with high speed on Nanyuki \(around 4 m s⁻¹\) while lower speed winds \(between 1 and 2 m s⁻¹\) from](#)
 1101 [a more variable directions \(between 170 and 300 degrees\) are blow in Nyeri preventing the possible dispersion of](#)
 1102 [pollutants.](#)

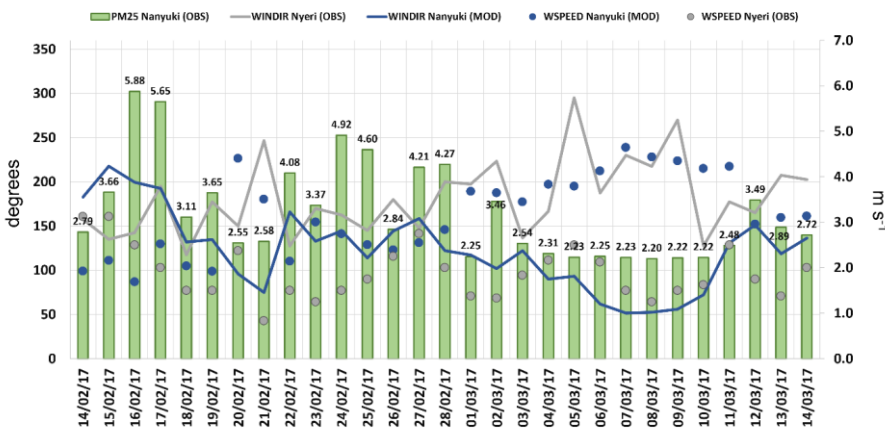
Deleted: 5

Deleted: 5

Deleted: northeastern

Deleted: 2

Deleted: 2



1103
 1104 **Figure 8:** Comparison between daily observed values of wind speed (grey spots) directions (grey lines) from the MIDAS site
 1105 of Nyeri (not in Figure 2c), modelled daily wind speed (blue dots) and directions (blue lines) from the site of Nanyuki with
 1106 daily average observations of PM_{2.5} (expressed in µg m⁻³, green columns) obtained from the sampling site of Nanyuki (red dot
 1107 in Figure 2c).

Deleted: .

Deleted: 3

Deleted: 3

1109 The present analysis was done on the relationships between weather conditions and the relative correspondence
 1110 in hourly and daily levels of PM_{2.5}. Further analyses are necessary to [clarify](#) the possible presence of additional or
 1111 alternative factors influencing the changes in concentrations observed and modelled by CHIMERE. The presence
 1112 of possible precipitations during the low concentration period could represent an alternative possibility the change

Deleted: investigate

1122 in concentrations. Despite this no precipitation were recorded during that period according to Pope et al. (2018)
1123 and no precipitation was modelled by WRF in that time period. Nevertheless, the lack of additional weather
1124 observations in the sampling site of Nanyuki and middle way between the two towns prevent from any additional
1125 hypothesis in relation to the presence of possible pollutant transport phenomena that will be object of future
1126 investigations. Further efforts will be oriented in a more detailed trajectory analysis of the winds and in a more
1127 detailed representation of the emissive sources present in the area to investigate possible transport effects in this
1128 area.

1129
1130 [The average concentrations of PM_{2.5} for the entire period of simulation between the 14th of February and 14th of](#)
1131 [March 2017 are shown for the domain centred over Kenya with spatial resolution of 2×2 km \(KEN2K, Figure 9\).](#)
1132 [Highest average concentrations during the monthly period are modelled in the urban area of Nairobi \(defined by](#)
1133 [the red dashed square in Figure 9\) with highest average values inside the city around 80 µg m⁻³. The concentrations](#)
1134 [are spread on average in the southwest area of the city and on the northeast side in direction of the conurbation of](#)
1135 [Thika and Makuyu. These towns became part of the Metropolitan Area of Nairobi in 2008 due to the rapid increase](#)
1136 [in population and urbanization of the area \(UNEP, 2009\) and represent a large hotspot of emissions of PM_{2.5} with](#)
1137 [concentrations modelled between 20 and 30 µg m⁻³ as average of the entire period. Other hotspots of concentration](#)
1138 [of PM_{2.5} found in the domain are the city of Nakuru with average concentrations between 20 and 40 µg m⁻³ and](#)
1139 [the area between Nyeri, Embu, Meru and Siakago with average concentrations around 20 and 30 µg m⁻³ \(Figure](#)
1140 [9\). The average of the modelled concentrations in the area of Nanyuki is generally smaller, with concentration not](#)
1141 [exceeding 10 µg m⁻³ in the whole area.](#)
1142

Deleted: nd

Deleted: j

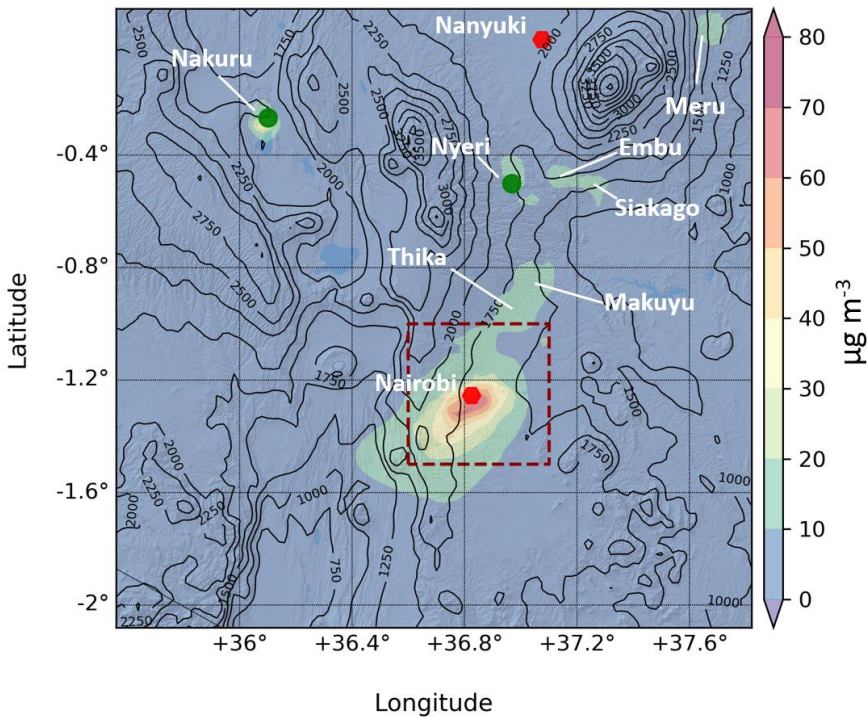


Figure 9: Average concentration of $PM_{2.5}$ for the whole simulated period for the domain KEN2K at spatial resolution of 2×2 km. The map shows the location of the hotspots with higher average concentrations modelled by CHIMERE for the entire period. The red dashed square shows the urban domain of Nairobi analysed for the Air Quality Indexes analysis in section 3.3.

3.3 CHIMERE as an Air Quality Management Tool

The usefulness of CHIMERE as a decision support tool to facilitate air quality management of large urban conurbations of SSEA was investigated for the three domains at a resolution of 2×2 km, namely: KEN2K, UGA2K and ETH2K. [Daily observations of \$PM_{2.5}\$ for the three domains were compared with modelled concentrations in terms of number of exceedances from the WHO limit of \$25 \mu g m^{-3}\$ observed and captured by the model \(Figure 10\). For the limited case of Nairobi, hourly average concentrations for the whole monitored period were compared with Air Quality Indexes data and the spatial distribution of daily average concentrations on the constituencies was analysed, highlighting how many areas of the city showed poor air quality indexes during the analysed period \(Figure 11\).](#)

Daily concentrations of $PM_{2.5}$ modelled by CHIMERE were compared with the number of exceedances of the WHO limit of $25 \mu g m^{-3}$ observed during the simulated period. Figure 10 shows the daily average concentrations

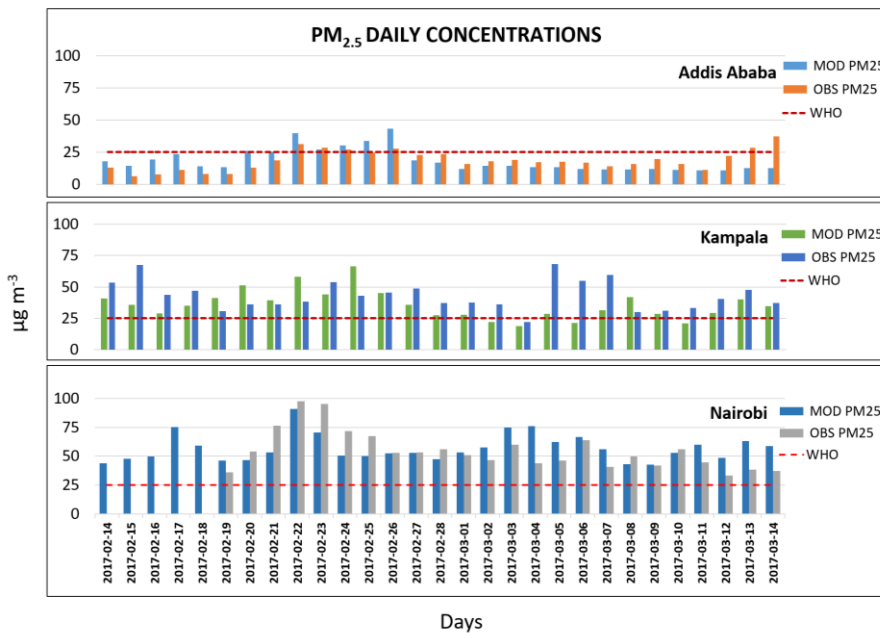
Deleted: ¶

Deleted: low

Deleted: (...)

Deleted:)

1168 for the three cities in the sampling sites used for the validation of the model. It can be seen that Nairobi and
 1169 Kampala have the highest number of exceedances from the WHO limits (24) followed by Addis Ababa with only
 1170 6 observed exceedances. From Table 6 it can be seen that CHIMERE provides sufficient accuracy to detect the
 1171 exceedances of PM_{2.5} from the WHO limits. In particular, it was able to detect 67 % of the exceedance for Addis
 1172 Ababa with only two false positives, 91 % for Kampala and all of the exceedances for Nairobi without any false
 1173 positives.



1174
 1175 **Figure 10:** Daily concentrations of PM_{2.5} between the 14th of February and 14th of March obtained from CHIMERE outputs
 1176 from domains at 2 × 2 km compared with U.S. Embassy daily totals for the cities of Addis Ababa (top) and Kampala (middle)
 1177 and with ASAP observations for the city of Nairobi (bottom). All three simulations have been compared also with the WHO
 1178 threshold limit for PM_{2.5} concentrations (red line). For the case of Nairobi, only observations from the 18th of February were
 1179 available.

1180 The Air Quality Index (AQI) represents the conversion of concentrations for fine particles such as PM_{2.5} to a
 1181 number on a scale from 0 to 500 (Table 6). The higher the AQI value, the greater the level of air pollution and the
 1182 greater the health concern. AQI values at or below 100 are generally thought of as satisfactory. When AQI values
 1183 are above 100, air quality is unhealthy: at first for certain sensitive groups of people (101 – 150), then for everyone
 1184 as AQI values get higher (> 151) (EPA, 2012).

1185
 1186
 1187 **Table 6:** Summary of the number of WHO exceeding limits for PM_{2.5} during the simulated period from the 14th of February to
 1188 the 14th of March 2017 observed and modelled.

Cities	Exceedances of WHO limits	
	(observed)	(modelled)
Nairobi	24	24
Addis Ababa	6	4
Kampala	24	22

Deleted: x

Deleted: 7)

Deleted: . Ratio between the observed and modelled Exceeding limit and number of model overestimations are also reported...

Deleted: WHO Exceeding Limits

Deleted: WHO Exceeding Limits

Deleted: Domains

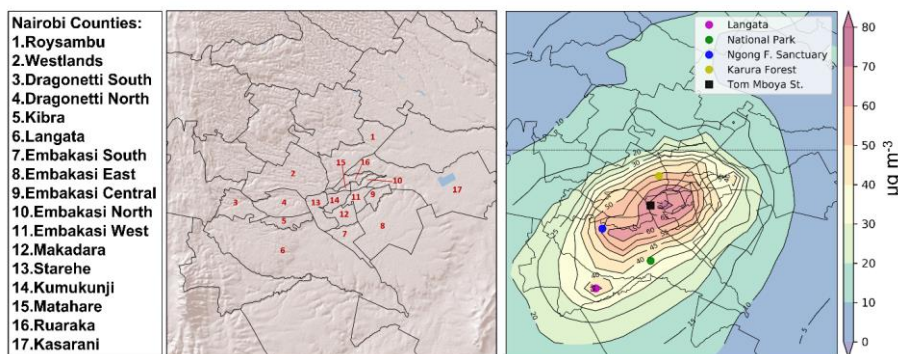
Formatted: Centered

Formatted Table

1197

1198 The daily average concentrations of $PM_{2.5}$ during the analysed period between the 14th of February and 14th of
 1199 March 2017 have been averaged for the urban area of Nairobi (red square in Figure 9 and Figure 11) and compared
 1200 with the city constituencies spatial extension according to data from the Open Africa dataset (Open-Africa, 2018).
 1201 According to the division, 17 are the constituencies inside the Nairobi city boundaries (Figure 11). Averaged daily
 1202 concentrations of $PM_{2.5}$ show that 8 of 17 constituencies had AQI values between 55.5-150.4 $\mu g m^{-3}$ during the
 1203 whole period. These areas are the most central and urbanized of Nairobi. Starehe constituency (n13 in Figure 11)
 1204 contains the Tom Mboya Street sampling site (black spot in Figure 11) previously discussed where the WHO
 1205 limits for $PM_{2.5}$ have been systematically exceeded during the analysed period. According to the SEDAC
 1206 population density data this area has population density between 15,000 and 30,000 people/km² exposed to AQI
 1207 between 151-200 corresponding to unhealthy category for human health. Finally, the Langata constituency
 1208 (magenta spot in Figure 11) has a population of 176,000 people and shows average levels of $PM_{2.5}$ of 45 $\mu g m^{-3}$,
 1209 unhealthy for sensitive groups of people.

Deleted:
 Deleted:
 Formatted: Superscript



1210
 1211 **Figure 11:** Map showing the urban area of the city of Nairobi shown as dashed square in Figure 9. The constituency division
 1212 of Nairobi (left) from Open Africa dataset (Open Africa, 2018) is compared with the average hourly concentrations of $PM_{2.5}$
 1213 over the analysed period (right).

Formatted: Font: 9 pt

1216 Moreover, Nairobi has a number of natural areas on the outskirts of city. Some particular locations such as the
 1217 Karura Forest (yellow spot in Figure 11) and the Ngong Forest Sanctuary (blue spot in Figure 11) show averaged
 1218 daily levels of $PM_{2.5}$ around 50 and 55 $\mu g m^{-3}$ corresponding to an AQI of between 101 and 150 (e.g., unhealthy
 1219 for certain sensitive groups of people). According to SEDAC data, the population density is between 10,000 and
 1220 15,000 people/km² in this area. Similarly, in the south side, near the entrance to the Nairobi National Park (1.36°
 1221 S, 36.82° E, green spot in Figure 11) the average daily levels of $PM_{2.5}$ are approximately 40 $\mu g m^{-3}$ with AQI
 1222 values between 101 and 150 with a population density around 10,000 people/km². This area (surface area 117
 1223 km²) has been impacted by a rapid urbanization since 1973 with a consequent increase of human activities
 1224 including settlement, pastoralism and agriculture (Ogega O.M., 2019). These activities have already made it
 1225 difficult for wildlife to migrate to and from the Nairobi National Park also are resulting in a deterioration of air
 1226 quality. The rapid increase of population density in the south side of Nairobi seriously risk increasing the level or
 1227 AQI exposing more people to harmful level of $PM_{2.5}$.

Deleted: Table 7: Air Quality Index categories and relative range of 24-hour average concentrations for $PM_{2.5}$ reported by the US EPA revised air quality standard for particle pollution of 2012 (EPA, 2012)†
 AQI Category

1235
1236
1237
1238
1239
1240
1241
1242
1243
1244
1245
1246
1247
1248
1249
1250
1251
1252
1253
1254
1255
1256
1257
1258
1259
1260
1261
1262
1263
1264
1265
1266
1267
1268
1269
1270
1271
1272
1273
1274

4 Conclusions

[The WRF and CHIMERE models were configured and validated to simulate the air quality levels of PM in Eastern Sub-Saharan African urban conurbations.](#)

In order to obtain updated anthropogenic emissions for 2017, the global EDGAR inventory and the DICE inventory for Africa were merged and spatially distributed using population density data for the year 2017 obtained by linear extrapolation.

WRF showed a variable capability in reproducing the main surface weather variables according to the different conditions of the three domains. A lower agreement between observations and the model was observed in Kampala for relative humidity and wind speed. The analysis was carried out on all surface meteorological stations available from the MIDAS network on a three-hourly basis. A further meteorological analysis extended to vertical profiles could reveal possible limitations of the model. However, the absence of vertical meteorological data limited the analysis and validation to ground level only.

CHIMERE was able to reproduce the daily levels of PM_{2.5} for the urban site of Nairobi as well as for the rural site of Nanyuki. The 69 % of the MFB values and 88 % of the MFE value were inside the highest confidence area for Nairobi and the 97 % and 99 % for Nanyuki attesting that the agreement between the observed and modelled data was sufficient to allow for quantitative analyses of daily average concentrations. Similar findings were also found for the other two urban background domains of Addis Ababa (57 % for MFB and 80 % for MFE) and Kampala (48% for MFB and 74 % for MFE) despite different characteristics and sources of observation being used for the validation. The discrepancies observed in the hourly trends of PM_{2.5} modelled by CHIMERE compared to observed values in the urban sites suggest that further studies are needed in the three urban areas. These studies are required to improve the understanding of the typology and quantity of local emission sources, which are sometimes misrepresented or absent in global emission inventories. This will enable the chemical processes acting in the urban troposphere to be adequately characterised and thereby actual air quality levels to be determined.

Nevertheless, using existing data sets, CHIMERE has shown reliability in reproducing both hourly and daily levels of PM_{2.5} with hourly values largely inside the range of reliability connected with mean fractional bias and error.

[The merged emission inventory DICE-EDGAR, despite the low resolution was able to return a correct magnitude for the emissions in representation of urban and rural context. Despite this, few urban peaks observed in Nairobi have been missed by CHIMERE or in other cases misrepresented highlighting the necessity of further efforts in the creation of newer emission inventories for SSEA. In the light of this, the possibility to develop local emission inventories, ideally at high spatial resolution it would represent a significant step ahead in the air quality research in this area of the world. Despite this and at the extent of the present data, CHIMERE showed enough robustness and reliability to be adopted as a decision support tool for the management of air quality, correctly reproducing most of the exceedances of the limits set by the WHO for PM_{2.5} for all three cities considered.](#)

Deleted: ¶

Deleted: patterns

1277 The analysis focused on the average concentrations of PM_{2.5} for the domain of Kenya revealed that the
1278 metropolitan area of Nairobi represents a big hotspot of air pollution but that also small cities located in the
1279 outskirts of the capital of Kenya showed worrying levels of atmospheric contamination. These levels of air
1280 pollution have the potential capability to affect also rural areas where the local emissions are rare or not present.
1281 The possibility of transport phenomena of PM_{2.5} towards these areas, however, is still to be verified. The work
1282 has also shown for urban area of Nairobi the presence of low and unhealthy air quality indexes in 8 of 17 its
1283 constituencies and the relative population density exposed to harmful level of air contamination. Moreover, a
1284 number of natural areas in the outskirts of Nairobi have similarly low levels of AQI and increasing population
1285 highlighting how the problem of poor urban air quality due to rapid urbanisation, anthropogenic activities and
1286 lack of regulation can also detrimentally affect and deteriorate natural habitats.

1287
1288 The present work represents a first step in the use of numerical models for atmospheric chemistry simulations in
1289 East Africa with particular focus on urban conurbation. The aim of the present work was to assess the possibility
1290 to perform simulations with results close to observations in order to open the road for more detailed works. The
1291 natural next step of the present research aims to refine the quantity and quality of the input data used for the
1292 validation of both modelling system in order to improve the reliability of the predictions. Moreover, a more
1293 detailed analysis of the secondary inorganic and organic components of PM_{2.5} will be conducted for the three
1294 domains. Finally, the performance of CHIMERE will be tested in the reproduction of gaseous species too in order
1295 to give a wider vision of the capabilities and opportunities of numerical modelling in this area of the world with
1296 present data. Additional future efforts to improve the calibration and validation of the modelling system, especially
1297 relating to meteorology, will focus on assessing the dispersion dynamics of contaminants through urban centres
1298 and possible pollution transport events from urban to rural areas. To aid this, further work is required by local
1299 East African authorities and research bodies to improve the quantity and the quality of data for weather and air
1300 quality simulations. However, in this work, we have shown that currently available data is sufficient to carry out
1301 simulations of air quality that can be used for quantitative evaluation of anthropogenic emissions impact and to
1302 support mitigation policies at the local level.

1303
1304 **Authors Contribution:** **Andrea Mazzeo:** Conceptualization, Methodology, Software, Validation, Writing-
1305 Original draft preparation, Writing- Reviewing and Editing. **Michael Burrow:** Supervision, Writing - Review &
1306 Editing **Andrew Quinn:** Supervision, Resources. **Eloise A. Marais:** Data curation, Resources, Writing - Review
1307 and Editing. **Ajit Singh:** Resources, **David N'gang'a:** Resources, **Michael Gatari:** Resources. **Francis Pope:**
1308 Supervision, Data curation, Funding acquisition, Writing - Review and Editing.

1309 **Acknowledgements:**

1311 The work is funded by the UK Department for International Development (DFID) via the EPSRC grant 'Digital
1312 Air Quality' (EP/T030100/1) and by the East Africa Research Fund (EARF) grant 'A Systems Approach to Air
1313 Pollution (ASAP) East Africa'. The practical support of the Schools of Geography and Earth Sciences and
1314 Engineering at the University of Birmingham are gratefully acknowledged.

1315

Formatted: Subscript

Deleted: F

Deleted:

Deleted: ¶

1319 **Data Availability:** the combined DICE-EDGAR anthropogenic emission inventory is downloadable from:
1320 <https://doi.org/10.25500/edata.bham.00000695>, CHIMERE model is downloadable from:
1321 <https://www.lmd.polytechnique.fr/chimere/> while WRF model is downloadable from:
1322 https://www2.mmm.ucar.edu/wrf/users/download/get_sources.html. Weather observations used for the validation
1323 of WRF have been downloaded from the Met Office:
1324 <http://catalogue.ceda.ac.uk/uuid/220a65615218d5c9cc9e4785a3234bd0>. Data relative to observations of PM_{2.5}
1325 for Nairobi (Kenya) are available upon request to the authors of Pope et al. (2018) while observations of PM_{2.5}
1326 for Addis Ababa (Ethiopia) and Kampala (Uganda) are available upon request to the respective U.S. Embassies.

Deleted:

Formatted: Font color: Text 1

Formatted: Subscript

Formatted: Subscript

1327 1328 **References**

- 1329 Alduchov O., E. R.: Improved Magnus Form Approximation of Saturation Vapor Pressure, *J. Of Appl.*
1330 *Met.*, 35, 601-609, [https://doi.org/10.1175/1520-0450\(1996\)035<0601:IMFAOS>2.0.CO;2](https://doi.org/10.1175/1520-0450(1996)035<0601:IMFAOS>2.0.CO;2), 1996.
- 1331 Amegah, A. K., and Agyei-Mensah, S.: Urban air pollution in Sub-Saharan Africa: Time for action,
1332 *Environ Pollut*, 220, 738-743, 10.1016/j.envpol.2016.09.042, 2017.
- 1333 Anav, A., Menut, L., Khvorostyanov, D., and VIOvy, N.: Impact of tropospheric ozone on the Euro-
1334 Mediterranean vegetation, *Global Change Biology*, 17, 2342-2359, 10.1111/j.1365-
1335 2486.2010.02387.x, 2011.
- 1336 Assamoi, E.-M., and Liousse, C.: A new inventory for two-wheel vehicle emissions in West Africa for
1337 2002, *Atmospheric Environment*, 44, 3985-3996, 10.1016/j.atmosenv.2010.06.048, 2010.
- 1338 Avis W. and Khaemba W.: Vulnerability and air pollution, 2018.
- 1339 Barnard, J.: An evaluation of the FAST-J photolysis algorithm for predicting nitrogen dioxide
1340 photolysis rates under clear and cloudy sky conditions, *Atmospheric Environment*, 38, 3393-3403,
1341 10.1016/j.atmosenv.2004.03.034, 2004.
- 1342 Bessagnet, B., Pirovano, G., Mircea, M., Cuvelier, C., Aulinger, A., Calori, G., Ciarelli, G., Manders, A.,
1343 Stern, R., Tsyro, S., García Vivanco, M., Thunis, P., Pay, M.-T., Colette, A., Couvidat, F., Meleux, F.,
1344 Rouïl, L., Ung, A., Aksoyoglu, S., Baldasano, J. M., Bieser, J., Briganti, G., Cappelletti, A., D'Isidoro, M.,
1345 Finardi, S., Kranenburg, R., Silibello, C., Carnevale, C., Aas, W., Dupont, J.-C., Fagerli, H., Gonzalez, L.,
1346 Menut, L., Prévôt, A. S. H., Roberts, P., and White, L.: Presentation of the EURODELTA III
1347 intercomparison exercise – evaluation of
- 1348 the chemistry transport models' performance on criteria pollutants and joint
- 1349 analysis with meteorology, *Atmospheric Chemistry and Physics*, 16, 12667-12701, 10.5194/acp-16-
1350 12667-2016, 2016.
- 1351 Bian, H., Prather, M.: Fast-J2: accurate simulation of stratospheric photolysis in global chemical
1352 models, *J. Atmos. Chem*, 41, 281–296, <https://doi.org/10.1023/A:1014980619462>, 2002.
- 1353 Bockarie, A. S., Marais, E. A., and MacKenzie, A. R.: Air Pollution and Climate Forcing of the Charcoal
1354 Industry in Africa, *Environ Sci Technol*, 54, 13429-13438, 10.1021/acs.est.0c03754, 2020.
- 1355 Boylan, J. W., and Russell, A. G.: PM and light extinction model performance metrics, goals, and
1356 criteria for three-dimensional air quality models, *Atmospheric Environment*, 40, 4946-4959,
1357 10.1016/j.atmosenv.2005.09.087, 2006.
- 1358 Brauer, M., Amann, M., Burnett, R. T., Cohen, A., Dentener, F., Ezzati, M., Henderson, S. B.,
1359 Krzyzanowski, M., Martin, R. V., Van Dingenen, R., van Donkelaar, A., and Thurston, G. D.: Exposure
1360 assessment for estimation of the global burden of disease attributable to outdoor air pollution,
1361 *Environ Sci Technol*, 46, 652-660, 10.1021/es2025752, 2012.
- 1362 Burroughs Peña, M. S., and Rollins, A.: Environmental Exposures and Cardiovascular Disease: A
1363 Challenge for Health and Development in Low- and Middle-Income Countries, *Cardiology Clinics*, 35,
1364 71-86, <https://doi.org/10.1016/j.ccl.2016.09.001>, 2017.

1366 Carter, W. P. L.: Development of the SAPRC-07 chemical mechanism, *Atmospheric Environment*, **44**,
1367 5324-5335, 10.1016/j.atmosenv.2010.01.026, 2010.

1368 Collins, W., Rasch, P., Boville, B., Hack, J., McCaa, J., Williamson, D., Kiehl, J., Briegleb, B., :
1369 Description of the NCAR Community Atmosphere Model (CAM 3.0). , NCAR Tech Notes, 2004.

1370 Crippa M., G. D., Muntean M., Shaaf E., Dentener F., van Aardenne J.A., Monni S., Doering U., Olivier
1371 J.G.J., Pagliari V. and Janssens-Maenhout G.: Gridded emissions of air pollutants for the period 1970-
1372 2012 within EDGAR v4.3.2, *Earth Sci. Data*, **10**, 1987 – 2013, <https://doi.org/10.5194/essd-2018-31>,
1373 2018.

1374 Dalal, S., Beunza, J. J., Volmink, J., Adebamowo, C., Bajunirwe, F., Njelekela, M., Mozaffarian, D.,
1375 Fawzi, W., Willett, W., Adami, H. O., and Holmes, M. D.: Non-communicable diseases in sub-Saharan
1376 Africa: what we know now, *Int J Epidemiol*, **40**, 885-901, 10.1093/ije/dyr050, 2011.

1377 deSouza P., N. V., Klopp J. M., Shaw B. E., Ho W. O., Saffell J., Jones R. and Ratti C.: : A Nairobi
1378 experiment in using low cost air quality monitors, *Clean Air Journal*, **27**, 12-42,
1379 <http://dx.doi.org/10.17159/2410-972X/2017/v27n2a6>, 2017.

1380 Egondi, T., Kyobutungi, C., Ng, N., Muindi, K., Oti, S., van de Vijver, S., Ettarh, R., and Rocklov, J.:
1381 Community perceptions of air pollution and related health risks in Nairobi slums, *Int J Environ Res*
1382 *Public Health*, **10**, 4851-4868, 10.3390/ijerph10104851, 2013.

1383 Revised Air Quality Standards for particle pollution and updates to the Air Quality Index (AQI):
1384 https://www.epa.gov/sites/production0-etrfgvy8ufiles/2016-04/documents/2012_aqi_factsheet.pdf
1385 2012.

1386 Gaita, S. M., Boman, J., Gatari, M. J., Pettersson, J. B. C., and Janhäll, S.: Source apportionment and
1387 seasonal variation of PM_{2.5} in a Sub-Saharan African city: Nairobi, Kenya, *Atmospheric*
1388 *Chemistry and Physics*, **14**, 9977-9991, 10.5194/acp-14-9977-2014, 2014.

1389 Gatari, M. J., Kinney, P. L., Yan, B., Sclar, E., Volavka-Close, N., Ngo, N. S., Mwaniki Gaita, S., Law, A.,
1390 Ndiba, P. K., Gachanja, A., Graeff, J., and Chillrud, S. N.: High airborne black carbon concentrations
1391 measured near roadways in Nairobi, Kenya, *Transportation Research Part D: Transport and*
1392 *Environment*, **68**, 99-109, 10.1016/j.trd.2017.10.002, 2019.

1393 Guenther, A., Karl, T., Harley, P., Wiedinmyer, C., Palmer, P., and Geron, C.: : Estimates of global
1394 terrestrial isoprene emissions using MEGAN (Model of Emissions of Gases and Aerosols from
1395 Nature), *Atmos. Chem. Phys.* **6**, 3181–3210, <https://hal.archives-ouvertes.fr/hal-00295995>, 2006.

1396 Hauglustaine, D. A., Hourdin, F., Jourdain, L., Filiberti, M. A., Walters, S., Lamarque, J. F., and Holland,
1397 E. A.: Interactive chemistry in the Laboratoire de Météorologie Dynamique general circulation
1398 model: Description and background tropospheric chemistry evaluation, *Journal of Geophysical*
1399 *Research: Atmospheres*, **109**, n/a-n/a, 10.1029/2003jd003957, 2004.

1400 Haywood, J. M., Pelon, J., Formenti, P., Bharmal, N., Brooks, M., Capes, G., Chazette, P., Chou, C.,
1401 Christopher, S., Coe, H., Cuesta, J., Derimian, Y., Desboeufs, K., Greed, G., Harrison, M., Heese, B.,
1402 Highwood, E. J., Johnson, B., Mallet, M., Marticorena, B., Marsham, J., Milton, S., Myhre, G.,
1403 Osborne, S. R., Parker, D. J., Rajot, J. L., Schulz, M., Slingo, A., Tanré, D., and Tulet, P.: Overview of
1404 the Dust and Biomass-burning Experiment and African Monsoon Multidisciplinary Analysis Special
1405 Observing Period-0, *Journal of Geophysical Research*, **113**, 10.1029/2008jd010077, 2008.

1406 Hong S., D. J., and Shu–Hua Chen S.: A revised approach to ice microphysical processes for the bulk
1407 parameterization of clouds and precipitation, *Mon. Wea. Rev.* **132**, 103-120,
1408 [https://journals.ametsoc.org/view/journals/mwre/132/1/1520-](https://journals.ametsoc.org/view/journals/mwre/132/1/1520-0493_2004_132_0103_aratim_2.0.co_2.xml)
1409 [0493_2004_132_0103_aratim_2.0.co_2.xml](https://journals.ametsoc.org/view/journals/mwre/132/1/1520-0493_2004_132_0103_aratim_2.0.co_2.xml), 2004.

1410 Hong S., N. Y., Dudhia J.: : A new vertical diffusion package with an explicit treatment of entrainment
1411 processes, *Mon. Wea. Rev.* **134**, 2318–2341,
1412 <https://journals.ametsoc.org/view/journals/mwre/134/9/mwr3199.1.xml>, 2006.

1413 Kerandi, N., Arnault, J., Laux, P., Wagner, S., Kitheka, J., and Kunstmann, H.: Joint atmospheric-
1414 terrestrial water balances for East Africa: a WRF-Hydro case study for the upper Tana River basin,
1415 *Theoretical and Applied Climatology*, **131**, 1337-1355, 10.1007/s00704-017-2050-8, 2017.

1416 Kerandi, N. M., Laux, P., Arnault, J., and Kunstmann, H.: Performance of the WRF model to simulate
1417 the seasonal and interannual variability of hydrometeorological variables in East Africa: a case study
1418 for the Tana River basin in Kenya, *Theoretical and Applied Climatology*, 130, 401-418,
1419 10.1007/s00704-016-1890-y, 2016.

1420 Kinney, P. L., Gichuru, M. G., Volavka-Close, N., Ngo, N., Ndiba, P. K., Law, A., Gachanja, A., Gaita, S.
1421 M., Chillrud, S. N., and Sclar, E.: Traffic Impacts on PM(2.5) Air Quality in Nairobi, Kenya, *Environ Sci*
1422 *Policy*, 14, 369-378, 10.1016/j.envsci.2011.02.005, 2011.

1423 Kume, A., Charles, K., Berehane, Y., Anders, E. and Ali, A.: Magnitude and variation of traffic air
1424 pollution as measured by CO in the City of Addis Ababa, Ethiopia, *Ethiopian Journal of Health*
1425 *Development*, 24, <https://doi.org/10.4314/ejhd.v24i3.68379>, 2010.

1426 Lacaux, J. P., Brustet, J.M., Delmas, R. et al.: Biomass burning in the tropical savannas of Ivory Coast:
1427 An overview of the field experiment Fire of Savannas (FOS/DECAFE 91), *J Atmos Chem*, 22, 195–216,
1428 <https://doi.org/10.1007/BF00708189>, 1995.

1429 Li, C., Martin, R. V., van Donkelaar, A., Boys, B. L., Hammer, M. S., Xu, J. W., Marais, E. A., Reff, A.,
1430 Strum, M., Ridley, D. A., Crippa, M., Brauer, M., and Zhang, Q.: Trends in Chemical Composition of
1431 Global and Regional Population-Weighted Fine Particulate Matter Estimated for 25 Years, *Environ Sci*
1432 *Technol*, 51, 11185-11195, 10.1021/acs.est.7b02530, 2017.

1433 Liousse, C., Guillaume, B., Grégoire, J. M., Mallet, M., Galy, C., Pont, V., Akpo, A., Bedou, M., Castéra,
1434 P., Dungall, L., Gardrat, E., Granier, C., Konaré, A., Malavelle, F., Mariscal, A., Mieville, A., Rosset, R.,
1435 Serça, D., Solmon, F., Tummon, F., Assamoi, E., Yoboué, V., and Van Velthoven, P.: Updated African
1436 biomass burning emission inventories in the framework of the AMMA-IDAF program, with an
1437 evaluation of combustion aerosols, *Atmospheric Chemistry and Physics*, 10, 9631-9646,
1438 10.5194/acp-10-9631-2010, 2010.

1439 Liousse, C., Assamoi, E., Criqui, P., Granier, C., & Rosset, R.: Explosive growth in African combustion
1440 emissions from 2005 to 2030, *Environmental Research Letters*, 9, [https://doi.org/10.1088/1748-](https://doi.org/10.1088/1748-9326/9/3/035003)
1441 [9326/9/3/035003](https://doi.org/10.1088/1748-9326/9/3/035003), 2014.

1442 Loosmore, G. A., and Cederwall, R. T.: Precipitation scavenging of atmospheric aerosols for
1443 emergency response applications: testing an updated model with new real-time data, *Atmospheric*
1444 *Environment*, 38, 993-1003, <https://doi.org/10.1016/j.atmosenv.2003.10.055>, 2004.

1445 Mailler, S., Menut, L., Khvorostyanov, D., Valari, M., Couvidat, F., Siour, G., Turquety, S., Briant, R.,
1446 Tuccella, P., Bessagnet, B., Colette, A., Létinois, L., Markakis, K., and Meleux, F.: CHIMERE-2017: from
1447 urban to hemispheric chemistry-transport modeling, *Geoscientific Model Development*, 10, 2397-
1448 2423, 10.5194/gmd-10-2397-2017, 2017.

1449 Marais, E. A., and Wiedinmyer, C.: Air Quality Impact of Diffuse and Inefficient Combustion Emissions
1450 in Africa (DICE-Africa), *Environ Sci Technol*, 50, 10739-10745, 10.1021/acs.est.6b02602, 2016.

1451 Marais, E. A., Silvern, R. F., Vodonos, A., Dupin, E., Bockarie, A. S., Mickley, L. J., and Schwartz, J.: Air
1452 Quality and Health Impact of Future Fossil Fuel Use for Electricity Generation and Transport in Africa,
1453 *Environ Sci Technol*, 53, 13524-13534, 10.1021/acs.est.9b04958, 2019.

1454 Markakis, K., Valari, M., Perrussel, O., Sanchez, O., and Honore, C.: Climate-forced air-quality
1455 modeling at the urban scale: sensitivity to model resolution, emissions and meteorology,
1456 *Atmospheric Chemistry and Physics*, 15, 7703-7723, 10.5194/acp-15-7703-2015, 2015.

1457 Mazzeo, A., Huneus, N., Ordoñez, C., Orfanos-Chequela, A., Menut, L., Mailler, S., Valari, M., van
1458 der Gon, H. D., Gallardo, L., and Muñoz, R.: Impact of residential combustion and transport
1459 emissions on air pollution in Santiago during winter, *Atmospheric Environment*, 190, 195-208, 2018.

1460 Mbewu, A., Mbanya, J.C., : Disease and Mortality in Sub-Saharan Africa, in: *Cardiovascular disease*
1461 edited by: Bank, W., 2006.

1462 MetOffice Integrated Data Archive System (MIDAS) Land and Marine Surface Stations Data (1853-
1463 current): <http://catalogue.ceda.ac.uk/uuid/220a65615218d5c9cc9e4785a3234bd0>, 2012.

1464 Nenes, A., Pilinis, C., Pandis, S.: : Isorropia: a new thermodynamic model for inorganic
1465 multicomponent atmospheric aerosols., *Aquat. Geochem*, 4, 123-152,
1466 <https://doi.org/10.1023/A:1009604003981>, 1998.

1467 Ngo, N. S., Gatari, M., Yan, B., Chillrud, S. N., Bouhamam, K., and Kinney, P. L.: Occupational
1468 exposure to roadway emissions and inside informal settlements in sub-Saharan Africa: A pilot study
1469 in Nairobi, Kenya, *Atmos Environ* (1994), 111, 179-184, 10.1016/j.atmosenv.2015.04.008, 2015.

1470 Ogega O.M., W. H. N., Mbugua J: Exploring the Future of Nairobi National Park in a Changing Climate
1471 and Urban Growth., in: *The Geography of Climate Change Adaptation in Urban Africa.*, edited by:
1472 Macmillan, P., 2019.
1473 [https://open.africa/dataset/kenya-administrative-boundaries/resource/b5bee56d-b7cb-4f23-8f2b-](https://open.africa/dataset/kenya-administrative-boundaries/resource/b5bee56d-b7cb-4f23-8f2b-356ca0044bf3)
1474 [356ca0044bf3](https://open.africa/dataset/kenya-administrative-boundaries/resource/b5bee56d-b7cb-4f23-8f2b-356ca0044bf3), 2018.

1475 Pai, S. J., Heald, C. L., Pierce, J. R., Farina, S. C., Marais, E. A., Jimenez, J. L., Campuzano-Jost, P., Nault,
1476 B. A., Middlebrook, A. M., Coe, H., Shilling, J. E., Bahreini, R., Dingle, J. H., and Vu, K.: An evaluation
1477 of global organic aerosol schemes using airborne observations, *Atmospheric Chemistry and Physics*,
1478 20, 2637-2665, 10.5194/acp-20-2637-2020, 2020.

1479 Parkin, D. M., Sitas, F., Chirenje, M., Stein, L., Abratt, R., and Wabinga, H.: Part I: Cancer in
1480 Indigenous Africans—burden, distribution, and trends, *The Lancet Oncology*, 9, 683-692,
1481 [https://doi.org/10.1016/S1470-2045\(08\)70175-X](https://doi.org/10.1016/S1470-2045(08)70175-X), 2008.

1482 Petkova, E. P., Jack, D. W., Volavka-Close, N. H., and Kinney, P. L.: Particulate matter pollution in
1483 African cities, *Air Quality, Atmosphere and Health*, 6, 603-614, [https://doi.org/10.1007/s11869-013-](https://doi.org/10.1007/s11869-013-0199-6)
1484 [0199-6](https://doi.org/10.1007/s11869-013-0199-6), 2013.

1485 Pohl, B., Crétat, J., and Camberlin, P.: Testing WRF capability in simulating the atmospheric water
1486 cycle over Equatorial East Africa, *Climate Dynamics*, 37, 1357-1379, 10.1007/s00382-011-1024-2,
1487 2011.

1488 Pope, F. D., Gatari, M., Ng'ang'a, D., Poynter, A., and Blake, R.: Airborne particulate matter
1489 monitoring in Kenya using calibrated low-cost sensors, *Atmospheric Chemistry and Physics*, 18,
1490 15403-15418, 10.5194/acp-18-15403-2018, 2018.

1491 Powers, J. G., Klemp, J.B., Skamarock, W.C., Davis, C.A., Dudhia, J., Gill, D.O., Coen, J.L., Gochis, D.J.,
1492 Ah madov, R., Peckham, S.E., Grell, G.A., Michalakes, J., Trahan, S., Benjamin, S.G., Alexander, C.R.,
1493 Di mego, G.J., Wang, W., Schwartz, C.S., Romine, G.S., Liu, Z., Snyder, C., Chen, F., Barlage, M.J., Yu,
1494 W., Duda, M.G.: : The weather research and forecasting model: overview, system efforts, and future
1495 directions, *Bull. Am. Meteorol. Soc.*, 98, 1717–1737, <https://doi.org/10.1175/BAMS-D-15-00308.1>,
1496 2017.

1497 Pun, B. K., Seigneur, C., and Lohman, K.: Modeling secondary organic aerosol formation via
1498 multiphase partitioning with molecular data, *Environ. Sci. Technol.*, 40, 4722–4731,
1499 <https://doi.org/10.1021/es0522736>, 2006.

1500 Real, E., and Sartelet, K.: Modeling of photolysis rates over Europe: impact on chemical gaseous
1501 species and aerosols, *Atmospheric Chemistry and Physics*, 11, 1711-1727, 10.5194/acp-11-1711-
1502 2011, 2011.

1503 Schwander, S., Okello, C. D., Freers, J., Chow, J. C., Watson, J. G., Corry, M., and Meng, Q.: Ambient
1504 particulate matter air pollution in Mpererwe District, Kampala, Uganda: a pilot study, *J Environ*
1505 *Public Health*, 2014, 763934, 10.1155/2014/763934, 2014.

1506 Seinfeld, J. H., Pandis, S.N.: *Atmospheric chemistry and physics: from air pollution to climate change*,
1507 edited by: Sons, J. W., 2016.

1508 Singh, A., Avis, W. R., and Pope, F. D.: Visibility as a proxy for air quality in East Africa, *Environmental*
1509 *Research Letters*, 15, 10.1088/1748-9326/ab8b12, 2020.

1510 Singh, A., Ng'ang'a, D., Gatari, M., Kidane, A. W., Alemu, Z., Derrick, N., Webster, M. J., Bartington, S.,
1511 Thomas, N., Avis, W. R., and Pope, F.: Air quality assessment in three East African cities using
1512 calibrated low-cost sensors with a focus on road-based hotspots, *Environmental Research*
1513 *Communications*, 10.1088/2515-7620/ac0e0a, 2021.

1514 Skamarock, W., Klemp, J., Dudhia, J., Gill, D., Barker, D., Duda, M., Huang, X., Wang, W., Powers, J., :
1515 A description of the advanced research WRF version 3. NCAR, 2008.

1516 Teklay, A., Dile, Y. T., Asfaw, D. H., Bayabil, H. K., and Sisay, K.: Impacts of land surface model and
1517 land use data on WRF model simulations of rainfall and temperature over Lake Tana Basin, Ethiopia,
1518 Heliyon, 5, e02469, 10.1016/j.heliyon.2019.e02469, 2019.

1519 Telford, P. J., Abraham, N. L., Archibald, A. T., Braesicke, P., Dalvi, M., Morgenstern, O., O'Connor, F.
1520 M., Richards, N. A. D., and Pyle, J. A.: Implementation of the Fast-JX Photolysis scheme (v6.4) into the
1521 UKCA component of the MetUM chemistry-climate model (v7.3), Geoscientific Model Development,
1522 6, 161-177, 10.5194/gmd-6-161-2013, 2013.

1523 Tewari, M., F. Chen, W. Wang, J. Dudhia, M. A. LeMone, K. Mitchell, M. Ek, G. Gayno, J. Wegiel, and
1524 R. H. Cuenca,: Implementation and verification of the unified NOAA land surface model in the WRF
1525 model. In Proceedings of the 20th Conference on Weather Analysis and Forecasting, 16th Conference
1526 on Numerical Weather Prediction, Seattle, 2004.

1527 Thompson A. M., W. J. C., Hudson R. D., Guo H., Herman J. R., and Fujiwara M.: Tropical tropospheric
1528 ozone and biomass burning Science, 291, 2128-2132, 10.1126/science.291.5511.2128, 2001.

1529 Trewhela, B., Huneus, N., Munizaga, M., Mazzeo, A., Menut, L., Mailler, S., Valari, M., and Ordoñez,
1530 C.: Analysis of exposure to fine particulate matter using passive data from public transport,
1531 Atmospheric Environment, 215, 116878, 2019.

1532 UN-Habitat New Urban Agenda <http://habitat3.org/wp-content/uploads/NUA-English.pdf>, 2017.

1533 United Nation World Population Prospect <https://population.un.org/wpp/>, 2019.

1534 City of Nairobi Environment Outlook: <https://wedocs.unep.org/handle/20.500.11822/8738>, 2009.

1535 FEWS NET: <https://fews.net/east-africa/seasonal-monitor/march-2022>, access: May 2022, 2022.

1536 Valari, M., and Menut, L.: Transferring the heterogeneity of surface emissions to variability in
1537 pollutant concentrations over urban areas through a chemistry-transport model, Atmospheric
1538 Environment, 44, 3229-3238, 10.1016/j.atmosenv.2010.06.001, 2010.

1539 Van Leer, B.: Towards the ultimate conservative difference scheme. V. A second-order sequel to
1540 Godunov's method. , Journal of Computational Physics, 32, 101-136, 10.1016/0021-9991(79)90145-
1541 1, 1979.

1542 van Loon, M., Vautard, R., Schaap, M., Bergström, R., Bessagnet, B., Brandt, J., Builtjes, P. J. H.,
1543 Christensen, J. H., Cuvelier, C., Graff, A., Jonson, J. E., Krol, M., Langner, J., Roberts, P., Rouil, L.,
1544 Stern, R., Tarrasón, L., Thunis, P., Vignati, E., White, L., and Wind, P.: Evaluation of long-term ozone
1545 simulations from seven regional air quality models and their ensemble, Atmospheric Environment,
1546 41, 2083-2097, 10.1016/j.atmosenv.2006.10.073, 2007.

1547 Vautard, R., Builtjes, P. H. J., Thunis, P., Cuvelier, C., Bedogni, M., Bessagnet, B., Honoré, C.,
1548 Moussiopoulos, N., Pirovano, G., and Schaap, M.: Evaluation and intercomparison of Ozone and
1549 PM10 simulations by several chemistry transport models over four European cities within the
1550 CityDelta project, Atmospheric Environment, 41, 173-188, 10.1016/j.atmosenv.2006.07.039, 2007.

1551 Vliet, V. E. a. K., P.: Impacts of roadway emissions on urban particulate matter concentrations in
1552 sub-Saharan Africa: new evidence from Nairobi, Kenya, Environmental Scientific letters, 2,
1553 <https://doi.org/10.1088/1748-9326/2/4/045028>, 2007.

1554 Voulgarakis, A., Savage, N. H., Wild, O., Carver, G. D., Clemitshaw, K. C., Pyle, J. A.: Upgrading
1555 photolysis in the PHOTOMCAT CTM: model evaluation and assessment of the role of clouds,
1556 Geoscientific Model Development, 2, 59-72, <https://doi.org/10.5194/gmd-2-59-2009>, 2009.

1557 World Bank Open Data: <https://data.worldbank.org/>, access: June 2022, 2022.

1558 WHO: WHO Air quality guidelines for particulate matter, ozone, nitrogen dioxide and sulfur dioxide,
1559 2005.

1560 WHO Burden of disease from ambient air pollution for 2012:
1561 http://www.who.int/phe/health_topics/outdoorair/databases/AAP_BoD_results_March2014.pdf
1562 access: April 2022, 2012.

1563 WHO Ambient Air Pollution: A global assessment of exposure and burden of disease:
1564 <http://www.who.int/phe/publications/air-pollution-global-assessment/en/> access: May 2022, 2016.

1565 Wild, O., Zhu, X., and Prather, J.: Fast-J: Accurate simulation of the in- and below cloud photolysis in
1566 tropospheric chemical models., *J. Atmos. Chem*, 37, 245-282,
1567 <https://doi.org/10.1023/A:1006415919030>, 2000.
1568 Wu, W.-S., Purser, R.J., Parrish, D.F., : Three-dimensional variational analysis with spatially
1569 inhomogeneous covariances., *Mon. Weather Rev.*, 130, 2905–2916, [https://doi.org/10.1175/1520-0493\(2002\)130<2905:TDVAWS>2.0.CO;2](https://doi.org/10.1175/1520-0493(2002)130<2905:TDVAWS>2.0.CO;2), 2002.
1570 Zhang, L., Gong, S., Padro, J., and Barrie, L.: A size-segregated particle dry deposition scheme for an
1571 atmospheric aerosol module, *Atmospheric Environment*, 35, 549-560,
1572 [https://doi.org/10.1016/S1352-2310\(00\)00326-5](https://doi.org/10.1016/S1352-2310(00)00326-5), 2001.
1573 Zyryanov, D., Foret, G., Eremenko, M., Beekmann, M., Cammas, J. P., D'Isidoro, M., Elbern, H.,
1574 Flemming, J., Friese, E., Kioutsioutkis, I., Maurizi, A., Melas, D., Meleux, F., Menut, L., Moinat, P.,
1575 Peuch, V. H., Poupkou, A., Razinger, M., Schultz, M., Stein, O., Suttie, A. M., Valdebenito, A., Zerefos,
1576 C., Dufour, G., Bergametti, G., and Flaud, J. M.: 3-D evaluation of tropospheric ozone simulations by
1577 an ensemble of regional Chemistry Transport Model, *Atmospheric Chemistry and Physics*, 12, 3219-
1578 3240, 10.5194/acp-12-3219-2012, 2012.
1579

1580